NASA CR-957

EXPERIMENTAL INVESTIGATION OF THE MIXING OF TWO PARALLEL STREAMS OF DISSIMILAR FLUIDS

By Richard L. Baker and Herbert Weinstein

Prepared under Grant No. NsG-694 by
ILLINOIS INSTITUTE OF TECHNOLOGY
Chicago, Ill.

for Lewis Research Center

NATIONAL AERONAUTICS AND SPACE ADMINISTRATION

For sale by the Clearinghouse for Federal Scientific and Technical Information
Springfield, Virginia 22151 – CFSTI price $3.00

FOREWORD

Research related to advanced nuclear rocket propulsion is described herein. This work was performed under NASA Grant NsG-694 with Mr. Maynard F. Taylor, Nuclear Systems Division, NASA Lewis Research Center as Technical Manager.

ABSTRACT

The mixing region between parallel streams of both similar and dissimilar fluids has been the subject of much investigation. However, a recent analytical study of this problem by the authors which is more complete than those made in the past, could not be adequately verified without additional experimental information.

In this work, velocity and density profiles for both homogeneous and heterogeneous systems were obtained. The range of density ratios was 1:1 to 7:1. The velocity ratio range was 1:1 to 5:1. Turbulence intensities were also measured for the homogeneous case. The experimental method was based on hot wire anemometry.

The data obtained agreed well with the analytical investigations in the literature.

TABLE OF CONTENTS

TABLE OF CONTENTS (Continued)

LIST OF TABLES

LIST OF ILLUSTRATIONS

LIST OF ILLUSTRATIONS (Continued)

LIST OF ILLUSTRATIONS (Continued)

LIST OF SYMBOLS

Symbol	Definition
b	Width of mixing region for velocity
c	Constant of proportionality, i.e., $b = cx$
c_i	Amplification or damping factor
c_r	Velocity of propagation of disturbance
C	Molar density
$\mathcal{D}$	Diffusivity
d	Width of mixing region for velocity
f	Dependent variable for laminar similarity solution
F	Dependent variable for turbulent similarity solution
g	Acceleration of gravity
J	Richardson number
J_i	Molar flux of component i
K	$1/Sc$
K'	$1/Sc^{(t)}$
l	Prandtl's mixing length
P	Pressure or power input to sensor
p	Fluctuating power
R	Reynolds number
t	Time
u	x-component of velocity
U	Reference velocity
v	y-component of velocity
w	Dependent variable = $\int f d\eta$
x	Rectangular coordinate

Symbol	Definition
y	Rectangular coordinate
α	Wave number
$1/\beta$	Reference length for density
ϵ	Eddy viscosity
ξ	Independent variable in turbulent similarity solution
η	Independent variable in laminar similarity solution
λ	Constant related to velocity ratio, i.e., $\lambda = (u_1 - u_2)/(u_1 + u_2)$
Γ	Constant related to density ratio, i.e., $\Gamma = (\rho_1 - \rho_2)/(\rho_1 + \rho_2)$
χ_1	Empirical constant
φ	Amplitude function
μ	Viscosity
ν	Kinematic viscosity
ρ	Density
τ_{xy}	Apparent turbulent shearing stress
Nu	Nusselt number
Pr	Prandtl number
Ri	Richardson number
Sc	Schmidt number

Subscripts

A	Component A
B	Component B
i	Component i
1	Refers to lighter fluid

Symbol	Definition
2	Refers to heavier component
x	x-component
y	y-component

Superscripts

—	Time average
*	Molar average
'	Fluctuating component
(t)	Turbulent

I. INTRODUCTION

The mixing of adjacent free jets has been investigated both analytically and experimentally for many years. However, a complete treatment for both similar and dissimilar fluids was never undertaken and could not be patched together from previous investigations. A complete analytical solution in the similarity region obtained by the authors in a parallel investigation to this one (67) necessitated an experimental investigation with parameter ranges beyond anything available in the literature to prove its validity. This investigation was undertaken for this purpose.

The object of this work was to obtain both velocity and density profiles in the mixing region between adjacent half jets of dissimilar fluids.

The variation in density ratio of the two fluids was larger than any previous investigation, ranging from one to eight and the velocity ratio ranged from one to five. Only the turbulent mixing region was investigated experimentally. The similar part of the mixing region was established in the apparatus and its range shown by turbulent intensity measurements.

II. BACKGROUND

II-1. Homogeneous Case

Experimental data for this case has been taken by Albertson,[14], Reichardt,[13] Liepmann and Laufer[12] and others [51,52]. Alberton, et. al. investigated the velocity profiles of a two inch slot jet issuing into stagnant air. Two zones of flow establishment were shown to exist. The initial zone, from the mouth of the jet to the point at which the mixing region has penetrated to the centerline of the jet, corresponds closely to flow in a half-jet.

The velocity profiles in this region were shown to be similar and a normal probability function was fitted to the data.

Reichardt obtained experimental data for a half-jet. He demonstrated the similarity of the velocity profiles at sufficient distances downstream and compared his experimental results with the theory of Goertler. He obtained a value of the empirical constant σ of 13.5

See Reference 67 for a complete discussion of the analysis of this type of flow and an explanation of these terms.

Liepmann and Laufer[12] conducted an extensive experimental study of the half-jet. They also demonstrated the similarity of the velocity profiles at sufficient distances downstream. However, they reported that the width of the initial mixing region was very narrow and that the flow was laminar in the first six inches of the mixing zone. They compared their data with the theoretical results of Tollmien and of Goertler. It will be recalled that the essential difference between the work of Tollmien and that of Goertler is in the expression used to represent the turbulent shear stress in the mixing region. Tollmien used Prandtl's mixing length hypothesis while Goertler used Prandtl's exchange coefficient hypothesis. Liepmann and Laufer demonstrated that their experimental results could be brought into reasonable agreement with the mean velocity distributions derived from either the theory of Tollmien or that of Goertler. However, turbulent stress measurements and back calculation of the mixing length and the exchange coefficient showed that both varied across

the mixing region. Thus, they concluded that neither Prandtl's mixing length hypothesis or exchange coefficient hypothesis adequately describes the turbulence characteristics of the mixing region. They showed that the microscale of turbulence is constant across the larger part of the mixing region. They obtained a value of Goertler's empirical constant σ of 11.0 compared to the value of 13.5 obtained by Reichardt.[50]

Kobashi[51] also obtained data for a turbulent two dimensional slot jet. He concluded that the mean velocity distribution and the turbulent shearing stress distribution are independent of the free stream turbulence intensity. However, the extent of the variation of the free stream turbulence intensity is not stated. It would appear from his graphs that the variation was from about two to five per cent.

Additional experimental data for this case has been taken by Sato.[52] His investigations were mainly concerned with the transition and turbulence characteristics of the mixing region. He investigated the transition phenomena in a half-jet with hot-wire anemometers. He used three boundary layer plates of different length so as to have Blasius type velocity profiles at various stages of development at the beginning of the mixing region. It was found that for a given free stream velocity, the transition distance increased as the length of the boundary layer plate was increased, i.e., the greater the development of the

Blasius velocity profile at the beginning of the mixing region, the greater the distance to the point of transition.

In the transition region, nearly sinusoidal fluctuations were observed. By placing two hot-wires several millimeters apart in the flow direction, a phase lag of the two sinusoidal waves was clearly observed. From this the wave velocity was determined and the value agreed quite well with the wave velocity predicted theoretically by Lessen[3] and by Lin.[7]

In a later work, Sato[53] investigated the effect of artificial excitation by sound on the transition. The effect of the excitation on the transition was found to be most pronounced when the frequency of the sound coincided with the frequency of the naturally excited sinusoidal velocity fluctuation. Sato further substantiated his previous conclusion that the sinusoidal velocity fluctuation found in the mixing region corresponds to the unstable disturbance in the linearized stability theory. He experimentally demonstrated that the small disturbances grow exponentially as long as their amplitudes remain small. Sato classified the flow field into four regions. They were

1. Laminar region with no velocity fluctuations.
2. Linear region where the two dimensional velocity fluctuations grow exponentially.
3. Non-linear region with non-linear interaction and three dimensional fluctuations.
4. Fully developed turbulent region.

II -2 Heterogeneous Case

There is very little experimental data available for this case. A limited amount of data has been taken for the three dimensional axi-symmetric case. (See Hauff[54]). It has been observed that the spread of the mixing region for density is wider than that for velocity. Much more data is needed.

Ellison and Turner[55] experimentally investigated turbulent entrainment in stratified flows. They flowed fresh water over salt water and reported a damping of the turbulence with increased density difference and a marked decrease in turbulent entrainment with increase in an appropriately defined Richardson number.

Minami[56] obtained data for the flow of salt water and fresh water in a sluice. He reported a decrease in the eddy viscosity and the eddy diffusivity with an increase in a gradient form Richardson number.

A related experiment dealing with turbulence in a density stratified shear flow was performed by Webster.[57] Density stratification was obtained by heating the air. Essentially linear temperature and velocity gradients were obtained in the wind tunnel through the use of grids. A decrease in the components of the turbulence intensity was reported with increase in a gradient form Richardson number. Also, the vertical component of the turbulence intensity was observed to decrease relative to the streamwise component at higher Richardson numbers. This fact was taken

as indicative of the suppression of vertical motions due to the gravity field. Webster also reported that the eddy viscosity and the eddy conductivity decreased with increasing Richardson number.

Okuda[58] investigated the velocity distribution at the interface between two liquids. Flowing fresh water over salt water he observed that the velocity in the upper liquid decreases fairly rapidly near the interface as if it were a solid plane. A calculated velocity distribution based on the formation of a thin intermediate layer and one dimensional flow showed fairly good accordance with the observed profile. It was found that the larger the viscosity of the lower fluid was, the lower the velocity near the interface would be.

Reichardt[59] obtained experimental data on the stability of flat plate boundary layers with density stratification. The measurements were made in a rectangular channel. Air passed through the channel in which the upper wall was heated by steam and the lower wall was cooled with water. Laminar and turbulent flows were observed and the data showed good agreement with the theory of Schlichting.[36]

III. EXPERIMENTAL

III-1 Description of Apparatus

The apparatus used for the experimental analysis consisted of a small plexi-glass wind tunnel, a pressure blower, a hot wire anemometer system, two calibrating sections, a metered air supply and a metered freon supply. The general arrangement of the apparatus is shown in Figure III-1.1.

III-1-1 Wind Tunnel and Blower

The wind tunnel was constructed of one-half inch plexi-glass. Because of the relatively high cost of the freons, it was necessary to keep the wind tunnel cross section small in order to avoid excessive costs. However, it was also desirable to have the aspect ratio high enough to insure two dimensional flow. Since these two factors were essentially in conflict with one another, it was necessary to affect a compromise. The inside dimensions of the wind tunnel were twelve inches in width and four inches in height. A stainless steel plate 0.018 inches thick was used to divide the tunnel into two twelve inch by two inch channels. The tunnel was made up of four sections. The sections were flanged and bolted together. The first section was eighteen inches in length and served as an inlet section. A perforated plate consisting of one-eighth inch holes in a thin piece of plexi-glass was placed between the flanges connecting section one with section two. This plate served to distribute the flow more evenly across the cross section.

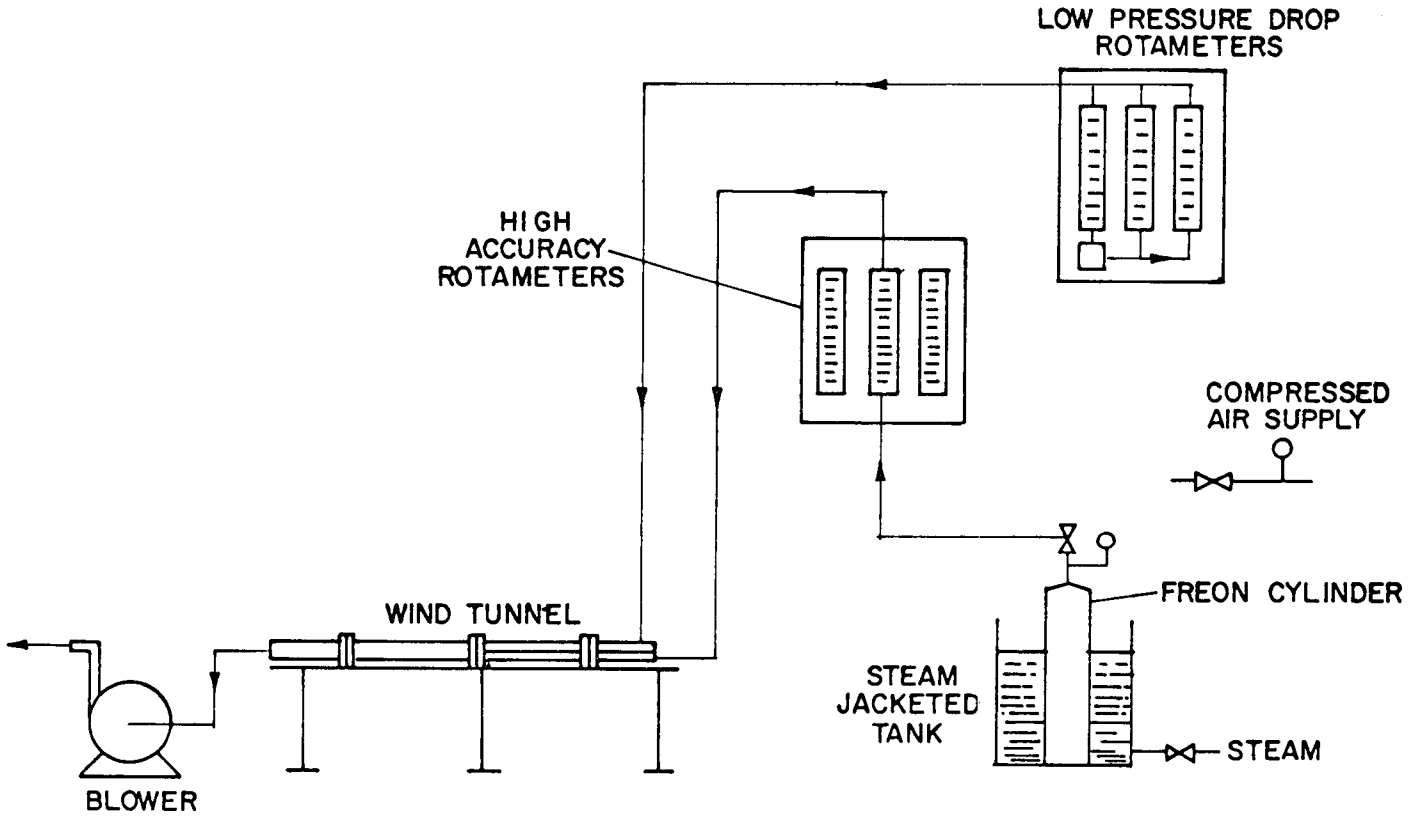

Fig.III-1.1 General Arrangement of Apparatus

The second section was thirty inches long. This section contained a twelve inch length of one-eighth inch mesh honeycomb and a series of screens in both the upper and the lower channel. The honeycomb served to dampen large scale turbulence and further distribute the flow evenly across the channel and between the upper and lower walls. Air-conditioning filter material was placed between the end of the honeycomb and the screens to further dampen turbulent fluctuations. A series of three screens was then used to reduce the turbulence intensity as low as possible without the use of a contraction. The screens were thirty mesh, sixty mesh and one-hundred mesh and were placed approximately one inch apart in that order. The honeycomb and screen placement was adjusted many times in order to achieve the lowest possible turbulence intensity together with a reasonably flat velocity profile.

The third section was thirty-six inches long and was the test section. A diagram of this section is shown in Figure III-1-1.1. A traversing mechanism was placed on the upper wall of this section. This mechanism allowed longitudinal and up and down movement of the hot-wire anemometer probes in a plane halfway between the sides of the tunnel. The stainless steel plate separating the two streams ended approximately three inches into this section. A pressure tap was placed near the end of this section in order to measure the static pressure in the test section.

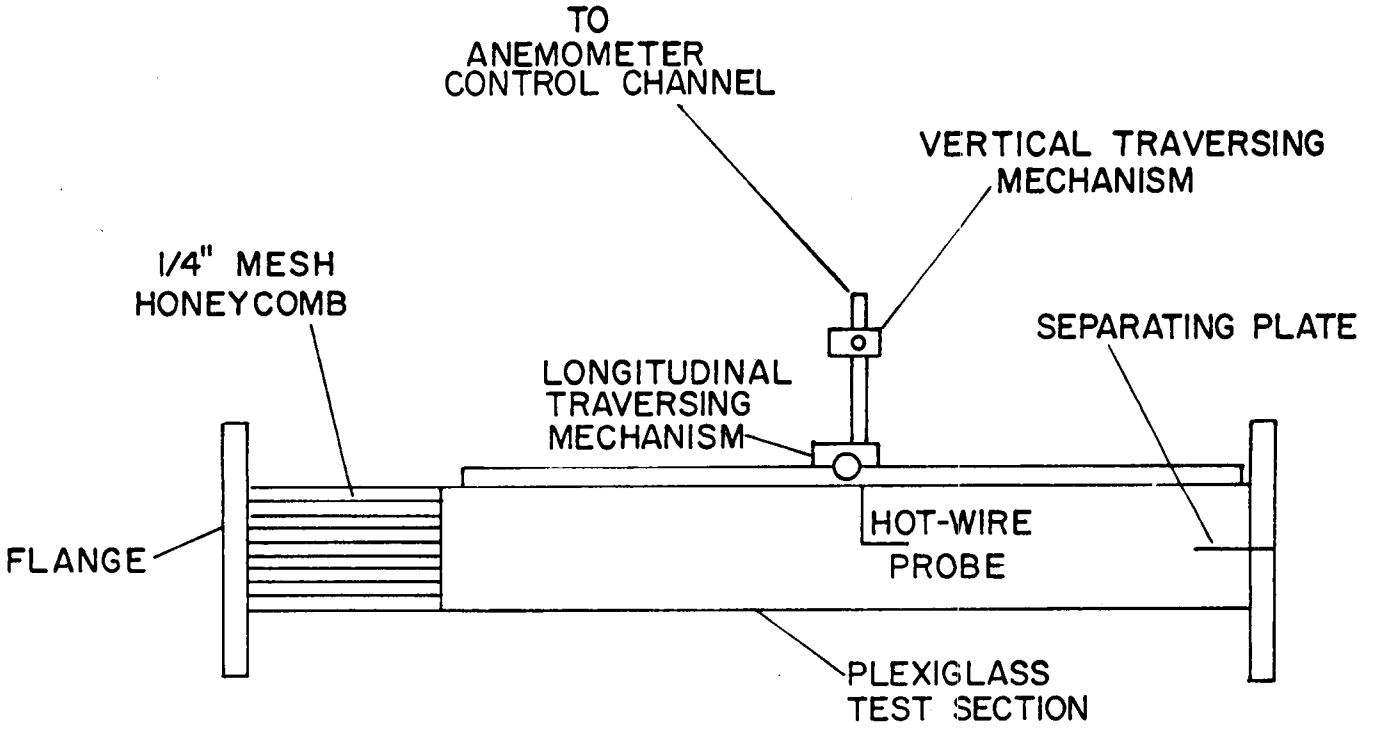

Fig. III-1-1.1 The Test Section

The fourth section was a converging outlet section eighteen inches long. This section was connected to the blower inlet through a transition piece and three inch diameter ducting. A six inch length of one-quarter inch mesh honeycomb was placed at the end of the test section to prevent disturbances in the outlet section from affecting the flow in the test section.

The blower was of the pressure blower type. It was powered by a 220 volt three horsepower motor and was rated at 100 cfm with a maximum suction head of twenty-seven inches of water.

Air entered the system through an air conditioning type filter and then passed through one of three rotameters in parallel. These rotameters were the low pressure drop type with an accuracy of two percent of the full scale reading. A butterfly valve was placed near the outlet of each rotameter in order to be able to throttle the flow to the desired flow rate. A gate valve was put in series with each butterfly valve in order to have one-hundred percent shut-off capability for any rotameter. From the gate valves the air passed directly to the inlet section of the wind tunnel.

III-1-2 Hot-Wire Anemometer System

The hot-wire anemometer equipment includes single wire probes, parallel wire probes, an aspirating probe, probe holders, angle adapters, two constant temperature control channels and related monitoring equipment. All of the hot-

wire anemometer equipment was purchased from Thermo-systems Incorporated in Minneapolis, Minnesota and was of the constant temperature type.

The sensors themselves were actually films and not wires. Each sensor consisted of a thin film of platinum on a quartz cylinder. One mil and two mil sensors were used with approximate lengths of 0.020 and 0.040 inches respectively. Ninety degree angle adapters were used so that the hot-film sensors could be placed into the mixing region in the configuration offering the least interference to the flow. The parallel wire probes consisted of two sensors mounted parallel to each other and approximately 0.020 inches apart. The single wire probes all had two mil sensors while the parallel wire probes had a one mil and a two mil sensor to obtain greater differences in their sensitivity.

The aspirating probe consisted of a one mil sensor mounted inside of a 0.080 inch ID tube. The tube was connected to a ninety degree angle adapter and probe holder and finally to a vacuum pump. The tube contained a jewel bearing with a hole diameter of 0.007 - 0.009 inches, behind the hot-film sensor. The vacuum pump reduced the pressure downstream from the bearing sufficiently to insure sonic velocity at the throat of the bearing. Since the sonic velocity varies with gas composition, the aspirating probe could be calibrated as an average concentration measuring device. The 0.007-0.009 inch throat diameter in the bearing was sufficiently small to insure that only a very small

percentage of the total flow passed through the aspirating probe.

It was possible to monitor either the power intput to the sensor or the bridge voltage from the constant temperature control channels. The monitoring equipment included a digital volt meter, an rms volt meter, a sum and difference unit and a dual beam oscilloscope. The power input to the sensor was monitored for calibration purposes and read as a voltage from the digital volt meter which was directly proportional to the sensor power input. The rms value of the fluctuating sensor power input was read from the rms volt meter as a rms voltage directly proportional to the rms power. The sum and difference unit supplied a signal which was the sum or the difference of the signals from both sensors of a parallel wire probe. With the dual beam oscilloscope it was possible to visually display two output signals at the same time for purposes of visualizing the fluctuating power or voltage due to fluctuating velocity and fluctuating density in the mixing region.

III-1-3 Calibrating Sections, Air and Freon Supply

The calibrating sections consisted of two seventeen foot lengths of pipe. The first was two inch standard iron pipe and the second was three-quarter inch stainless steel pipe. The reason that two calibrating sections were used was that this was necessary in order to obtain the desired calibrating velocities for the full range of concentration with the rotameters available. Three high

accuracy (± 1% of the instantaneous reading) rotameters were used for calibrating purposes and for metering the freon supply to the wind tunnel.

Air for calibrating purposes was taken from the building's compressed air supply. The air was scrubbed and filtered before passing it through a high accuracy rotameter to the gas mixing device. The freons were supplied as a liquid in large cylinders. Since it was necessary to vaporize the liquid freon, a means of supplying the latent heat of evaporation was needed. To accomplish this the freon cylinders were placed in a steam jacketed tank partly filled with water. The vaporized freon passed from the cylinder to the gas mixing device through a high accuracy rotameter.

The gas mixing device consisted of three two inch pipe couplings with two inch to one inch bushings in each end. The couplings with the bushings were connected by short one inch nipples. A two inch tee with bushings was connected to one of the end couplings. All three couplings and the tee were packed with brass scouring pads. For those calibrations which required the mixing of freon and air, the metered air and freon entered the tee and then passed on through the couplings.

III-2 Hot-wire Anemometer Techniques

III-2-1 Fundamental Relationships

Heat transfer from small heated cylinders was first studied extensively in connection with hot-wire anemometry

by King.[63] Many other investigations of this problem have been undertaken since that time.[64,65,66] It is well established that the heat transferred from the sensor can be represented by an expression of the form

$$P = [A + BV^n][T_s - T_e] \qquad \text{III-2-1.1}$$

where A, B and n are numerical constants, V is the velocity past the sensor, T_s is the temperature of the sensor and T_e is the temperature of the environment. The constant n is usually taken to be one-half. An equation of this form adequately describes the power input versus velocity characteristics for hot-wire anemometers so long as the velocity is sufficiently high. If the velocity is very low, the power loss versus square root of velocity curve becomes non-linear. This occurs below a velocity of about one foot per second for most gases.

Each investigator's results may be put into the form of equation III-2-1.1. The difference in the analyses lies in the expressions for A and B. The following empirical relationship was given by Kramers[65] and is widely used.

$$Nu = 0.42\ Pr^{0.2} + 0.57\ Pr^{1/3}\ Re^{0.5} \qquad \text{III-2-1.2}$$

In this expression, Nu is the Nusselt number, Pr is the Prandtl number and Re is the Reynolds number. When this heat transfer relationship is put into the form of equation III-2-1.1, the constants A and B are given by

$$A = 0.42 \frac{e\pi k_f \ell}{\alpha_1 R_o} (Pr)_f^{0.20} \qquad \text{III-2-1.3}$$

$$B = 0.57 \frac{e\pi k_f \ell}{\alpha_1 R_o} (Pr)_f^{1/3} \left(\frac{\rho_f d}{\mu_f} \right)^{0.5} \qquad \text{III-2-1.4}$$

In these expressions, e is a conversion constant, k is the thermal conductivity, μ is the viscosity, ρ is the density, α_1 is the linear temperature coefficient of electrical resistivity, R_o is the wire resistance at a reference temperature T_o, ℓ is the wire length, d is the wire diameter and the subscript f means that the quantity is evaluated at the film temperature. The film temperature is usually taken as the average of the sensor temperature T_s and the temperature of the environment T_e. Thus, the constants A and B depend upon the physical properties of the surrounding medium as well as the dimensions of the wire.

In actual practice, the factors A and B are determined experimentally. Once a calibration has been obtained, it is possible to back calculate an equivalent length and diameter using equations III-2-1.3 and III-2-1.4. The effect of physical properties on A and B can then be estimated. However, this technique is not reliable enough to allow determination of the values of A and B for a second gas based on the physical properties of that gas and the equivalent length and diameter obtained from the calibration of the wire in air.

The real utility of hot-wire anemometers is in the measurement of turbulent properties such as turbulence intensity and turbulent shearing stress. The velocity past the sensor V is assumed to be made up of an average stream velocity U and fluctuating components u' and v' in the flow direction and perpendicular to the flow direction respectively. Thus

$$V = \sqrt{(U + u')^2 + v'^2} \qquad \text{III-2-1.5}$$

The quantity V^n may be expanded in a Taylor series to give

$$V^n = U^n\left[1 + n\frac{u'}{U} + \frac{n(n-1)}{2}\frac{u'^2}{U^2} + \frac{n}{2}\frac{v'^2}{U^2} + \dots\right] \qquad \text{III-2-1.6}$$

with the assumptions

$$u' \ll U$$
$$v' \ll U \qquad \text{III-2-1.7}$$

equation III-2-1.6 may be linearized to give

$$V^n = U^n\left[1 + n\frac{u'}{U}\right] \qquad \text{III-2-1.8}$$

This expression may then be substituted into equation III-2-1.1 to give the instantaneous power supplied to the sensor

$$P = \overline{P} + p = \left[A + BU^n\left(1 + n\frac{u'}{U}\right)\right]\left[T_s - T_e\right] \qquad \text{III-2-1.9}$$

where $\overline{P}$ is the average power level and p is the small variation about the average power level caused by the fluctuating velocity u'. The average power level $\overline{P}$ is defined as

$$\overline{P} = [A + BU^n][T_s - T_e) \qquad \text{III-3-1.10}$$

and the power level at zero velocity P_o is defined by

$$P_o = A[T_s - T_e) \qquad \text{III-3-1.11}$$

Equations III-2-1.9, III-2-1.10 and III-2-1.11 may be combined to give

$$\frac{p/n}{\overline{P} - P^o} = \frac{u'}{U} \qquad \text{III-2-1.12}$$

Since the average values of p and u' are zero, the root mean square (rms) values are normally used as a measure of turbulence. Defining $\sqrt{\overline{u'^2}}$ as the root mean square value of u' and $\sqrt{\overline{p^2}}$ as the root mean square value of p, equation III-2-1.12 may be written

$$\frac{\sqrt{\overline{p^2}}}{\overline{P} - P_o} = \frac{\sqrt{\overline{u'^2}}}{U} \qquad \text{III-2-1.13}$$

The quantity on the right hand side of this equation is known as the turbulence intensity. Thus, the turbulence intensity of the fluctuating component of the velocity in the mean flow direction may be easily calculated from this relationship.

Equation III-2-1.12 may be obtained in a different manner. Differentiating equation III-2-1.1 gives

$$dP = nBV^{n-1}\, dV(T_s - T_e) \qquad \text{III-2-1.14}$$

Assuming that the fluctuating power p and the fluctuating velocity u' may be substituted for dP and dV respectively

and using equations III-2-1.5 and III-2-1.7, equation III-2-1.14 may be written

$$p = \frac{nBU^n u'}{U} \qquad \text{III-2-1.15}$$

This equation may then be combined with equations III-2-1.10 and III-2-1.11 to give equation III-2-1.12. The reason that two methods of deriving equation III-2-1.12 are given here is that the first method shows that the turbulence intensity calculated from this equation is for the fluctuating velocity in the mean flow direction while the second method of derivation is somewhat simpler and will be used in connection with turbulence measurements in a heterogeneous system.

If the composition of the fluid flowing past the hot-wire is variable, then the A and B in equation III-2-1.1 will no longer be constant since they depend on the physical properties of the surrounding medium. The power input to the hot-wire will depend upon the concentration C or the density ρ as well as the velocity past the sensor. The total derivative of the power input to the sensor may be written

$$dP = \left(\frac{\partial P}{\partial \rho}\right)_V d\rho + \left(\frac{\partial P}{\partial V}\right)_\rho dV \qquad \text{III-2-1.16}$$

Differentiation of equation III-2-1.1 shows that

$$\left(\frac{\partial P}{\partial \rho}\right)_V = \left[\frac{dA}{d\rho} + V^n \frac{dB}{d\rho}\right](T_s - T_e)$$

$$\left(\frac{\partial P}{\partial V}\right)_P = nBV^{n-1} dV (T_s - T_e) \qquad \text{III-2.1.17}$$

Substituting the fluctuating power p, the fluctuating velocity

u' and the fluctuating density ρ' for dP, dV and d_ρ respectively and combining equations III-2-1.17, III-2-1.16, III-2-1.11 and III-2-1.10 gives

$$p = R'\rho' + S'u' \qquad \text{III-2-1.18}$$

where

$$R' = [\frac{dA}{d\rho} + V^n \frac{dB}{d\rho}][T_s - T_e] \qquad \text{III-2-1.19}$$

and

$$S' = n(\bar{P} - P_o)(T_s - T_e)/V \qquad \text{III-2-1.20}$$

Alternatively, equation III-2-1.16 may be written

$$p = R''\rho' + S'' u' \qquad \text{III-2-1.21}$$

where

$$R'' = (\frac{\Delta P}{\Delta \rho})_V \qquad \text{III-2-1.22}$$

and

$$S'' = (\frac{\Delta P}{\Delta V})_\rho \qquad \text{III-2-1.23}$$

The method of calculating the turbulence intensity and the fluctuating density from these relationships is given in Section III-2-3.

III-2-2 Calibration Procedures

The calibration of the hot-wire anemometer equipment included calibration of the aspirating probe, single wire probes and parallel wire probes. During a calibration, the outlet of the calibrating section being used was placed inside of a plexi-glass chamber thirty-six inches long and

six inches by six inches in cross section. This was to avoid disturbance of the flow profiles in the calibrating section by convection currents in the room. The up and down part of the traversing mechanism was mounted on top of this chamber so that the probes could be easily held and centered during calibrations. If freon was to be used in the calibration, the water in the steam jacketed tank containing the freon cylinder was heated to about 105°F. After connecting the compressed air supply and the freon cylinder to the gas mixing device through the proper high accuracy rotameters and connecting the outlet of the gas mixing device to the calibrating section, the system was ready to begin a calibration.

The aspirating probe was calibrated by placing it in either calibrating section since the output of this probe does not depend on the approach velocity. After turning on the vacuum pump, the average power input to the hot-film in the aspirating probe was recorded from the digital volt meter for various concentrations of freon and air ranging from pure air to pure freon. Data was taken at nine intermediate concentrations for freon 12 and at four intermediate concentrations for freon C318. The calibration curve for freon 12 and air is shown in Figure III-2-2.1.

The following general calibration procedure was used for the hot-film sensors. A hot-film probe was placed in both calibrating sections, one at a time, and calibrated by flowing air in laminar flow past it at known flow rates.

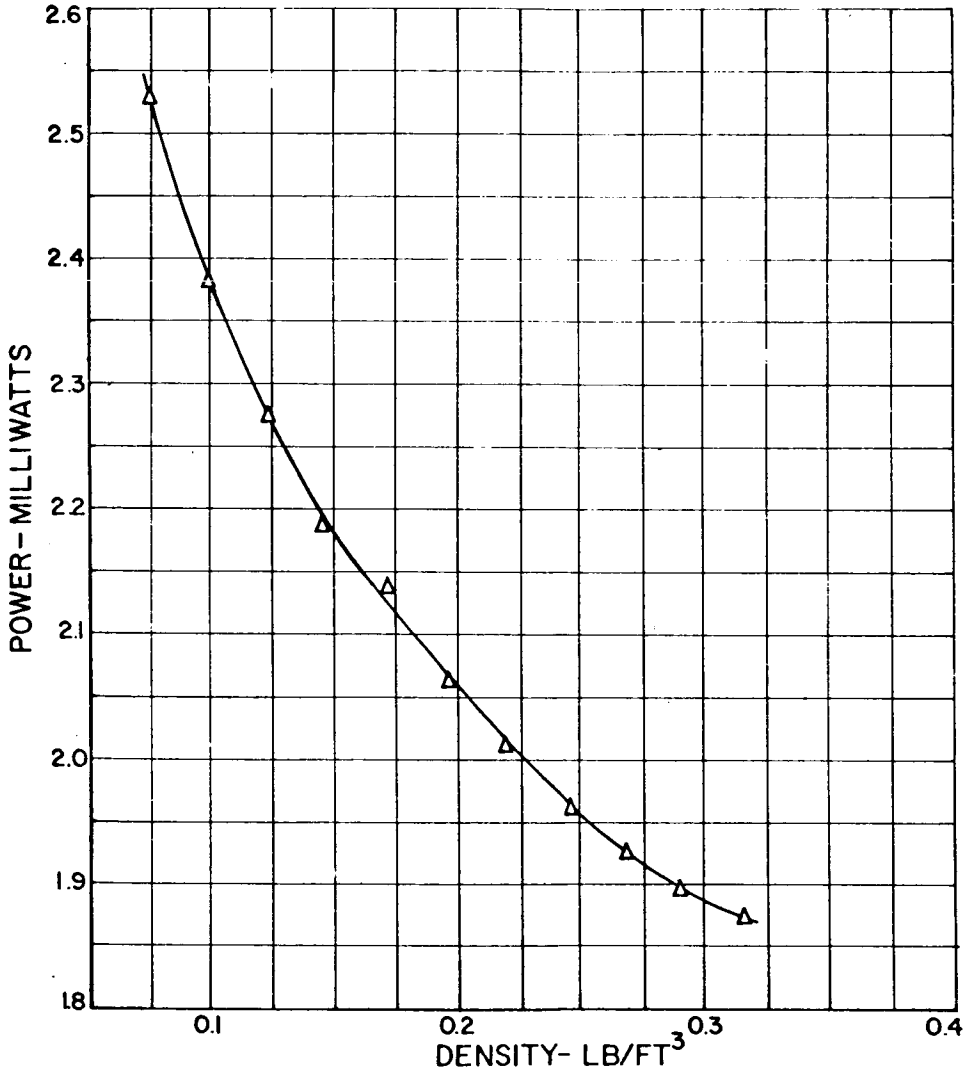

Fig. III-2-2.1 Aspirating Probe Calibration Curve for Freon 12 and Air

The calibration was obtained by placing the sensor on the centerline of the pipe and assuming that the velocity as that point was twice the average velocity in the pipe as for the parabolic velocity distribution for laminar flow in a pipe. The average power versus square root of velocity curves were then plotted from these calibrations. Very reasonable straight line calibration curves were obtained.

To obtain calibration curves for freon and air mixtures, additional procedures were necessary since a wide range of velocities for laminar flow of mixtures was not possible with the available rotameters. With a probe on the centerline of a calibrating section, air was put through it for a relatively wide range of turbulent Reynolds numbers. At each Reynold's number, the power input to the sensor was recorded. From this data and the previously obtained calibration curves for laminar flow, the ratio of average velocity to centerline velocity for that calibrating section was obtained for each Reynold's number. It was then assumed that this ratio was constant for a given value of the Reynold's number for all concentrations of freon and air flowing in that calibrating section. Power input readings were taken with a probe on the centerline and the flow at a Reynold's number for which the ratio of average velocity to centerline velocity was known. Data was taken for pure freon and for four intermediate concentrations between pure air and pure freon. In this way, calibration curves of power input versus the square root of velocity were obtained for pure

freon and the four intermediate concentrations. Two calibration curves for a single wire probe are shown in FigureIII-2-2.2. Calibration curves for each sensor of a parallel wire probe were similarly obtained.

III-2-3 Calculation Procedures

For the case of homogeneous flow, the average velocities were calculated directly from a power input reading from a single wire probe and the calibration curve for that wire. Likewise, the turbulence intensity for homogeneous flow was calculated directly from equation III-2-1.13 assuming that n was equal to one-half.

For the case of heterogeneous flow, the calculation procedure was somewhat more involved. From a set of calibration curves for mixtures of various densities, the slope and the intercept were plotted as a function of density. A smooth curve was then drawn through the points. Typical curves showing the slope B and the intercept A as a function of density are shown in Figure III-2-2.3. Graphs like this were prepared for a single wire probe and for both sensors of a parallel wire probe.

The first step in the calculation procedure was then to obtain the average density at each data point from the aspirating probe power input and the calibration curve for the aspirating probe. Next, the slope and the intercept of the calibration curve for the single wire probe for each density across the mixing region were obtained from a graph such as FigureIII-2-2.3. Knowing the slope

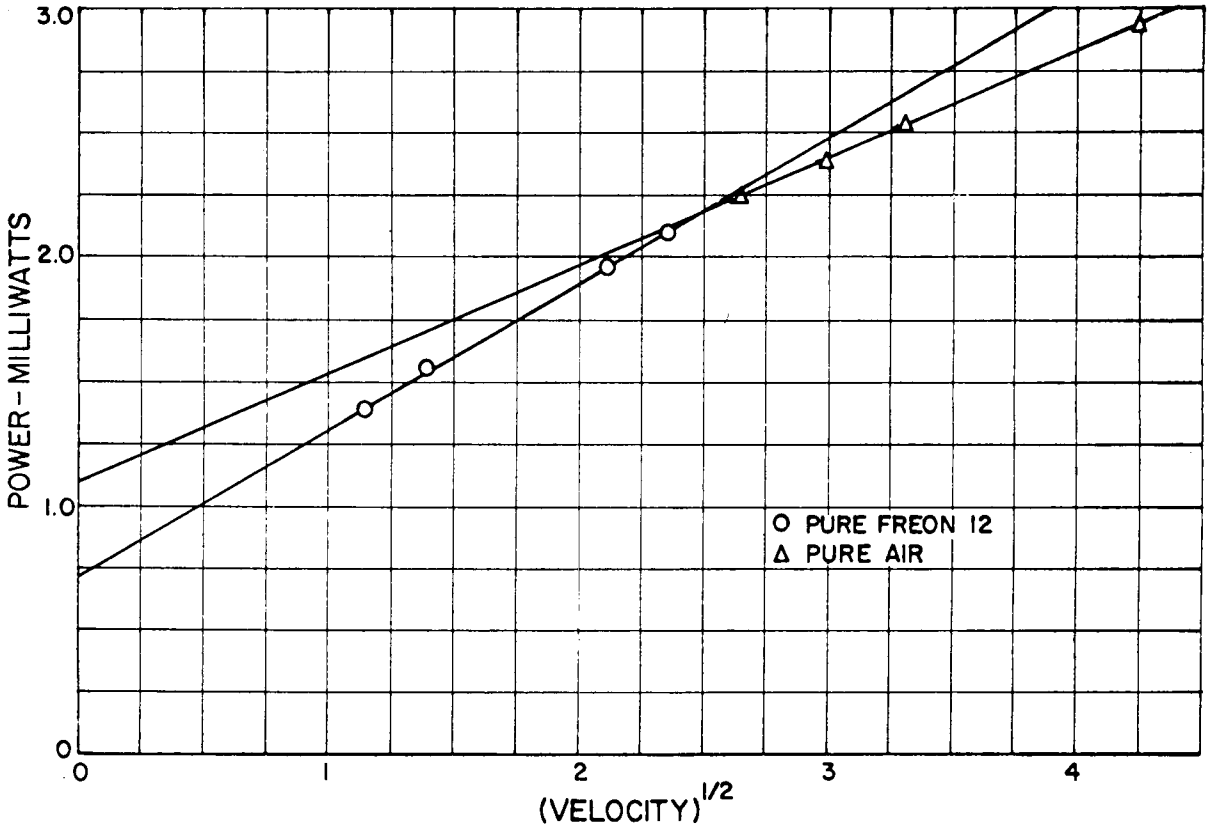

Fig.III-2-2.2 Calibration Curves of Single Wire Probe

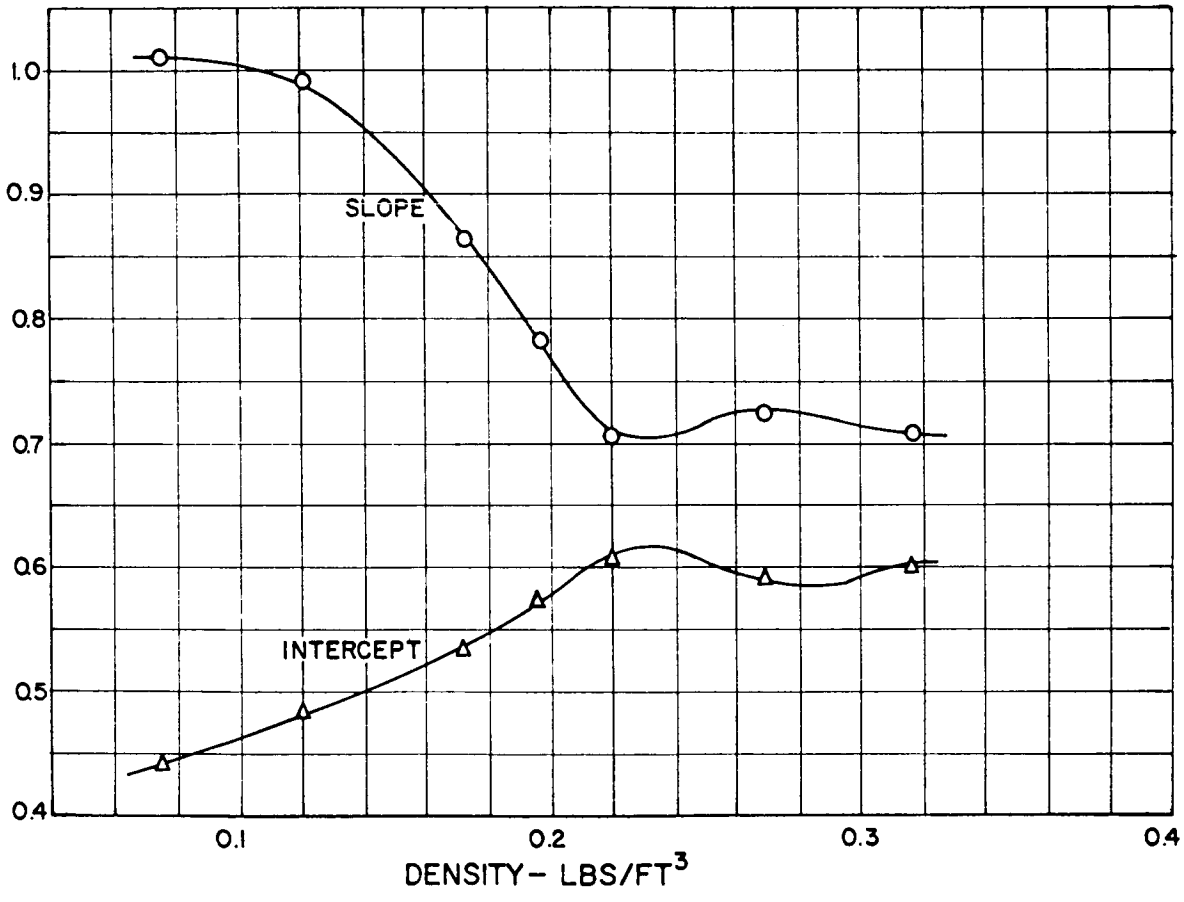

Fig. III-2-2.3 Slope "B" and Intercept "A" as a Function of Density

and the intercept of the calibration curve at each data point along with the sensor power input, the average velocity profiles were then calculated.

To obtain the turbulence intensity and other turbulence properties, the slope and intercept versus density curves for both sensors of a parallel wire probe were fitted with n-th degree polynomials. This was accomplished by using the SINPAK routine available on the IIT 7040 IBM computer. This routine determins the best polynomial fit to the data. It first fits the data with a Fourier sine series. This is then rearranged into a Chebychef series and this is finally rearranged into an n-th order polynomial. The degree of the polynomial in each case is determined by truncating the Fourier sine series and the Chebychef series at the point where the coefficients begin to display random noise. Polynomial coefficients for the curves of slope and intercept as a function of density were stored in the computer for each sensor of a parallel wire probe.

It would have been possible to differentiate these polynomials to obtain R' in equation III-2-1.19 and then to use equation III-2-1.18 for the calculation of the turbulence properties. However, a slightly different procedure employing equation III-2-1.21 was used.

Squaring both sides of equation III-2-1.21 and then averaging gives

$$\overline{p^2} = R''^2\,\overline{\rho'^2} + 2R''S''\,\overline{\rho' u'} + S''^2\,\overline{u'^2} \qquad \text{III-2-3.1}$$

The coefficients R" and S" are given by equations III-2-1.21 and III-2-1.23. These coefficients were calculated in the following way. The average density and the average velocity at a data point were first determined as outlined above. The density was then incremented by $\pm 0.05\ \rho$ and the sensor power input was calculated at each new density, for the same velocity, by means of the stored polynomials representing the slope and intercept versus density curves. R" was then calculated from

$$R'' = \left(\frac{\Delta P}{\Delta \rho}\right)_V = \frac{P(\rho+0.05\rho,V) - P(\rho-0.05\rho,V)}{0.10\rho} \qquad \text{III-2-3.2}$$

Combining equations III-2-1.23 and III-2-1.1, S" is given by

$$S'' = \left(\frac{\Delta P}{\Delta V}\right)_\rho = \left(\frac{\partial P}{\partial V}\right)_\rho = nBV^{n-1}\ (T_s - T_e) \qquad \text{III-2-3.3}$$

Since a polynomial representing B as a function of density was available, S" could be easily calculated.

An equation like equation III-2-3.1 may be written for the output from each sensor of a parallel wire probe and for an output which is the sum of the outputs from the two sensors. Three equations are then available which may be solved simultaneously for the three unknowns $\overline{\rho'^2}$, $\overline{\rho' u'}$ and $\overline{u'^2}$. Once these quantities have been determined, the turbulence intensity may be easily calculated by taking the square root of $\overline{u'^2}$ and dividing by the average velocity U. Likewise, the fluctuating density

$$\frac{\sqrt{\overline{\rho'^2}}}{\bar{\rho}} \qquad \text{III-2-3.4}$$

may be obtained by taking the square root of $\sqrt{\overline{\rho'^2}}$ and dividing by the average density. Finally, the correlation coefficient

$$\frac{\overline{\rho'u'}}{\sqrt{\overline{\rho'^2}}\,\sqrt{\overline{u'^2}}} \qquad \text{III-2-3.5}$$

may be calculated from $\overline{\rho'u'}$ and the previously determined quantities.

III-3 Operating Procedure and Data

Data was obtained for air mixing with air as well as air mixing with freon 12 and freon C318. Four runs were made in the homogeneous case. These were for λ values of 0.2, 0.4, 0.6, and 0.8 corresponding to velocity ratios of 3 to 2, 7 to 3, 4 to 1 and 9 to 1. For air mixing with freon 12, data was taken for λ values of 1/3, 0.6 and 0.8 corresponding to velocity ratios of 2 to 1, 4 to 1 and 9 to 1. For air mixing with freon C318, data was taken for $\lambda = 0.75$ only corresponding to a velocity ratio of 7 to 1.

III-3-1 Homogeneous Case

The operating procedure for this case was as follows. A calibrated single wire probe was placed in the test section. The blower was then turned on and the butterfly valves were adjusted to obtain the desired velocity ratio.

The velocity in each channel was obtained from a digital volt meter reading proportional to the sensor power input and the calibration curve for that sensor corrected for the difference between the tunnel pressure and the calibration pressure. The zero positions for downstream and vertical measurements were then obtained. The zero for downstream measurements were obtained by visual observation. The zero for vertical measurements was obtained by placing the sensor approximately one-eighth of an inch from the end of the plate separating the two streams and moving it up and down until a minimum power input reading was obtained. The accuracy of the vertical position measurements was ± 0.005 inches and the accuracy of the downstream position measurements was ±0.010 inches. The measurements were taken from scales having 0.020 inch scale divisions.

Once the proper velocity ratio was obtained and the zero positions had been determined, the data for the initial velocity distributions in the upper and the lower channels was taken. Data was taken at increments of 0.10 inches. Average and rms power readings were then taken for the calculation of the free stream turbulence intensity in each stream. Next, traverses were made across the mixing region at downstream positions of 2 inches, 4 inches, 8 inches and 13 inches. At 2 inches and 4 inches downstream, data was taken at increments of 0.050 inches. At 8 inches and 13 inches downstream data was taken at increments of 0.10 inches. The data taken at each position consisted of an average power reading and an rms power reading.

III-3-2 Heterogeneous Case

In this case, a single wire probe and the aspirating probe were placed in the test section at the same time. Both probes were connected to ninety degree angle adapters. Two or three cylinders of freon were then placed in the steam jacketed tank and the water in the tank was heated to about 105°F. The zero positions for the single wire probe were obtained in the same manner as in the homogeneous case. For the aspirating probe, the zero positions for both vertical and downstream position measurements were obtained visually.

After the zero positions for both probes had been obtained, the blower was turned on and the butterfly valves were adjusted to give the approximate desired flow rate in the upper channel. Next, the freon was brought into the lower channel inlet section from the freon cylinders in parallel through a high accuracy rotameter. The rotameter was set to give the approximate cfm needed for the desired velocity in the lower channel. The flow rates in the upper and the lower channels were then adjusted to give the desired velocity ratio. Data for the initial velocity distributions in the upper and the lower channel was then taken at increments of 0.20 inches. Average and rms power readings were taken for the calculation of the free stream turbulence intensity in each stream. The power input to the aspirating probe sensor was recorded with the probe in each stream in order to have pure component readings.

Next, traverses were made across the mixing region at four downstream positions with both probes. All data from the aspirating probe was taken at increments of 0.10 inches. For the single wire probe data was taken at increments of 0.050 inches for the first two downstream positions and at increments of 0.10 inches for the other two downstream positions. The data consisted of an average power reading and an rms power reading from the single wire probe and an average power reading from the aspirating probe.

The blower and the freon flow were then turned off. The single wire probe and the aspirating probe were removed from the test section and replaced with a parallel wire probe. The zero positions for the parallel wire probe were obtained visually. The blower and the freon flow were then turned on again. Traverses were made at the same downstream positions as with the single wire probe and the aspirating probe. Data was taken at the same vertical positions as with the other probes except that larger increments were taken in order to save time. At each position, three rms power readings were recorded. These were the outputs from the one mil and the two mil sensors and the sum of the two outputs taken from the sum and difference unit.

IV. RESULTS AND DISCUSSION

IV-1 Experimental

IV-1-1 Homogeneous Case

Velocity profiles and turbulence intensity profiles for various free stream velocity ratios are presented in Figs. IV-1-1.1 thru IV-1-1.10 for the λ values of 0, 0.2, 0.4, 0.6 and 0.8. The corresponding velocity ratios are 1 to 1, 3 to 2, 7 to 3, 4 to 1 and 9 to 1 respectively.

For each case the initial turbulence intensity in the upper stream was less than one percent. In the lower stream, the initial turbulence intensity was one or two percent at high velocity ratios, i.e., when the free stream velocity was quite low.

In each instance, there are two factors, in addition to the velocity ratio, which affect the velocity and turbulence intensity profiles in the mixing region. These factors are the boundary layers on the plate which initially separates the two streams and the boundary layers which build up on the upper and lower walls of the wind tunnel and accelerate the flow at the outer edges of the mixing region.

Figure IV-1-1.1 shows the velocity profiles initially and at downstream positions of two inches, four inches, eight inches and thirteen inches for the case in which the two free stream velocities are equal, i.e., $\lambda = 0$. It

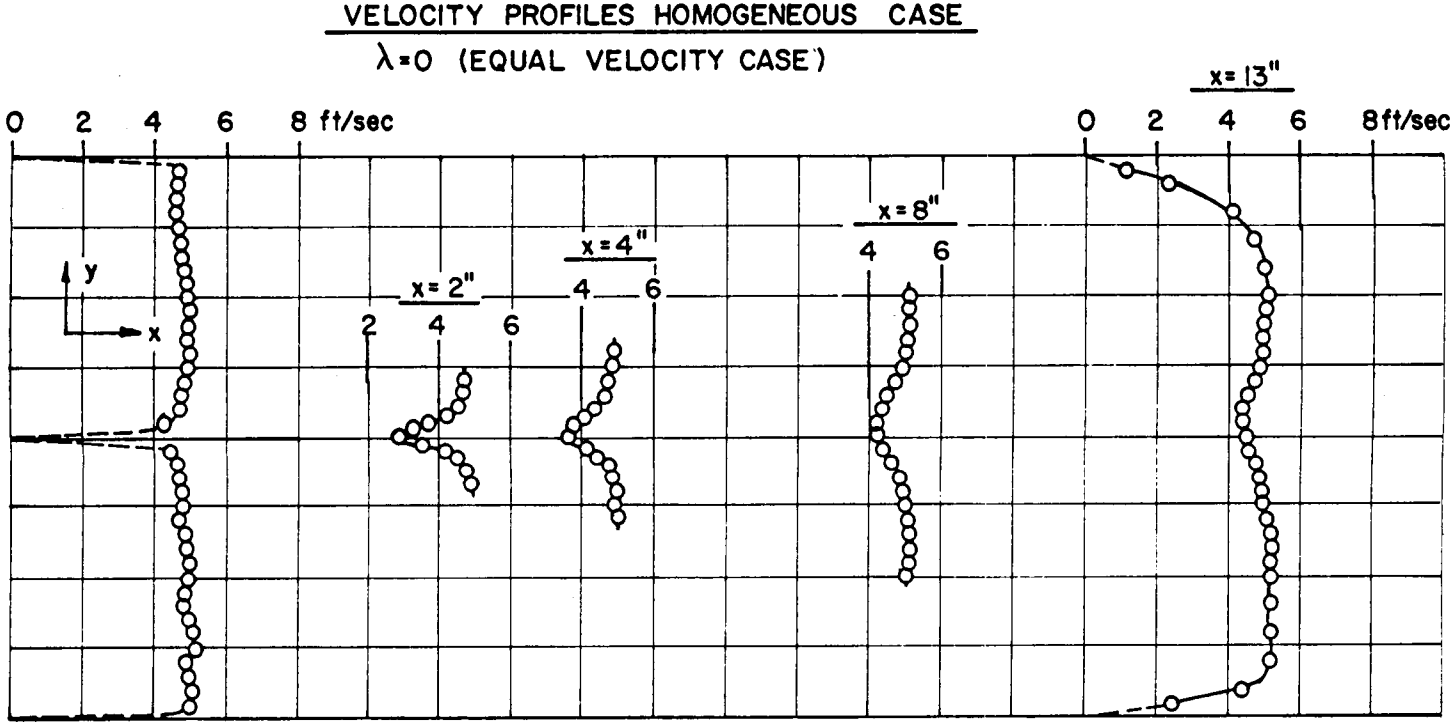
VELOCITY PROFILES HOMOGENEOUS CASE
λ=0 (EQUAL VELOCITY CASE)
0 2 4 6 8 ft/sec
y
x
x= 2"
2 4 6
x= 4"
4 6
x= 8"
4 6
x= 13"
0 2 4 6 8ft/sec

Fig. IV-1-1.1

can be seen that the effect of the boundary layers on the plate initially separating the two streams is still evident as a velocity decreement in the velocity profile thirteen inches downstream. The extent of the boundary layer development on the upper and lower walls of the wind tunnel is also shown.

This particular case corresponds closely to the problem of the wake of a flat plate at zero incidence. This is evidenced by the shape of the velocity profiles in Figure IV-1-1.1 and also by the turbulence intensity profiles shown in Figure IV-1-1.2 It will be noted that the turbulence intensity profiles at downstream positions of one-half inch and two inches exhibit peak values on both sides of the center line. Sato pointed out that this is a characteristic of the turbulence intensity in the wake of a flat plate at zero incidence and is due to the two inflection points in the wake velocity profile. The same explanation for this characteristic may be given here even though the initial velocity profiles before mixing are not of the Blasius type as in Sato's experiment. At the downstream positions of four inches, eight inches and thirteen inches, the width of the region in which the turbulence intensity is greater than the free stream value increases while the maximum value of the turbulence intensity decreases.

The initial and downstream velocity profiles for the case of $\lambda = 0.2$ are shown in Figure IV-1-1.3. Here again the effect of the boundary layers on the separating plate

TURBULENCE INTENSITY PROFILES HOMOGENEOUS CASE

λ=0 (EQUAL VELOCITY CASE)

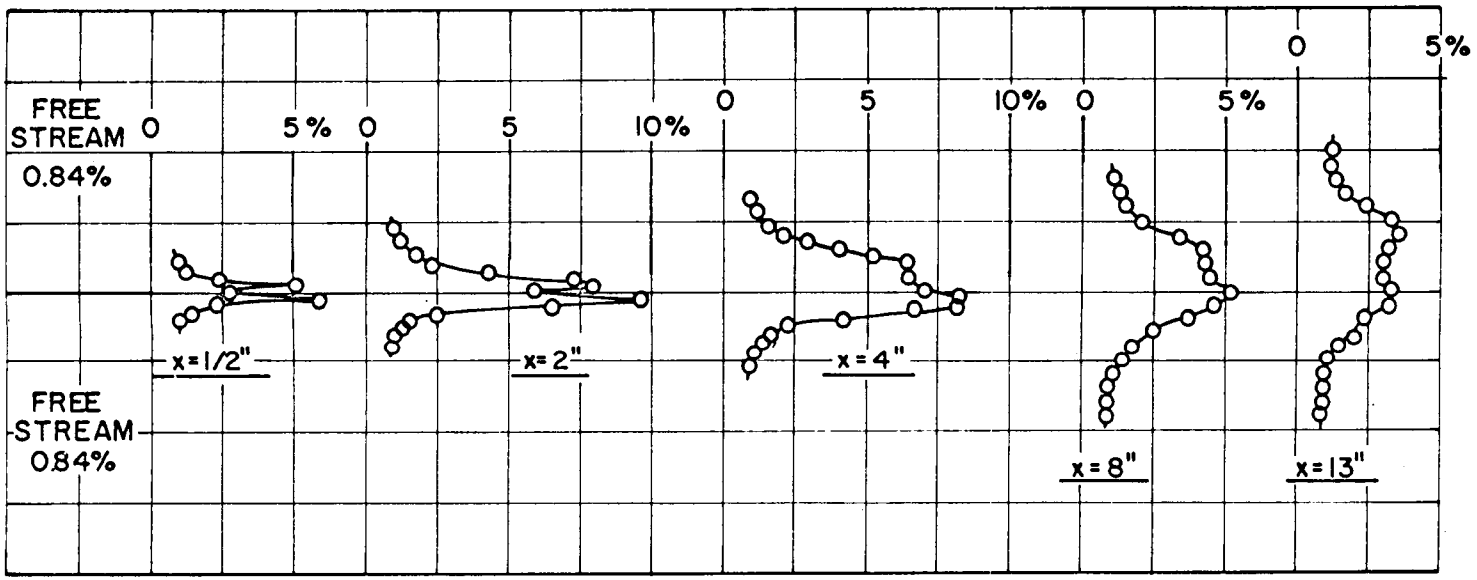

Fig. IV -1-1.2

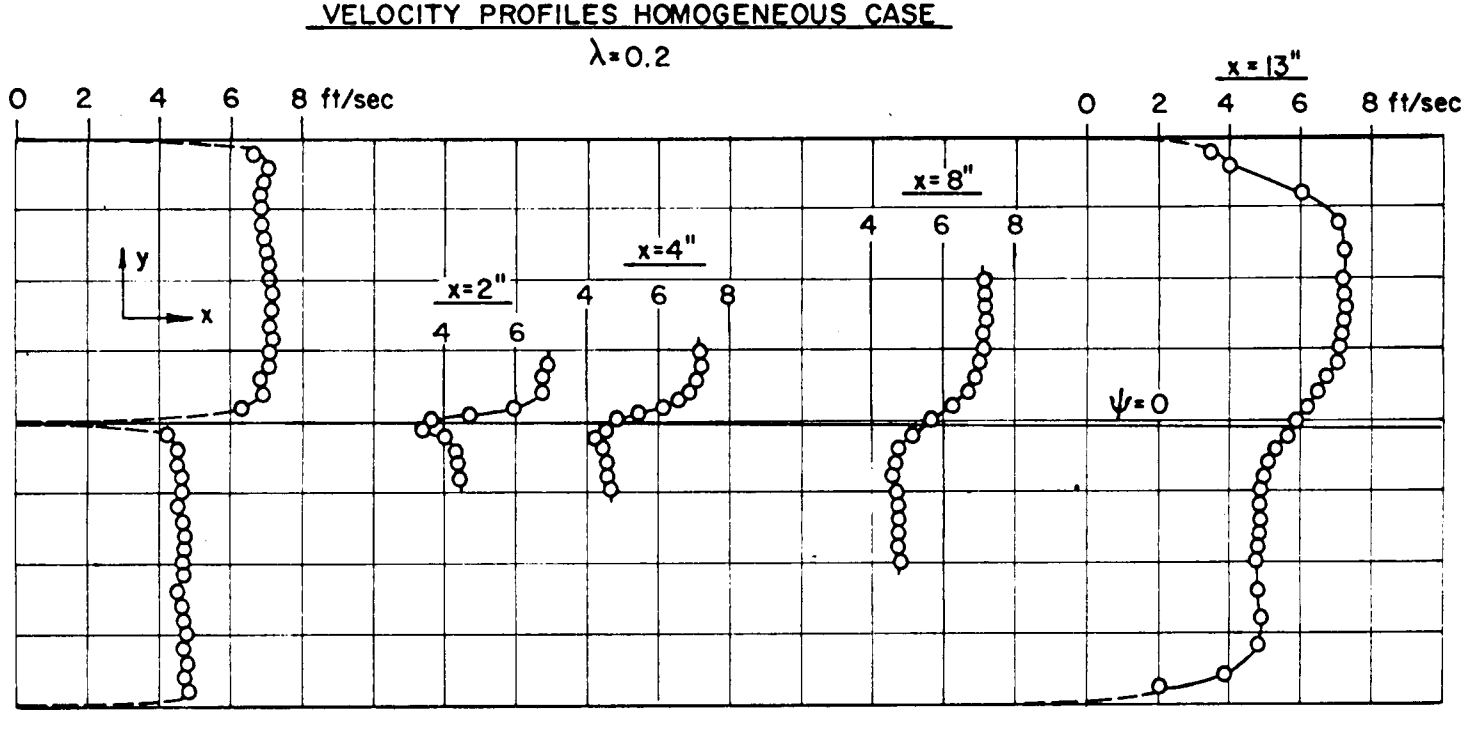
VELOCITY PROFILES HOMOGENEOUS CASE
λ=0.2
0 2 4 6 8 ft/sec
y
x
x=2"
4 6
x=4"
4 6 8
x=8"
4 6 8
x=13"
0 2 4 6 8 ft/sec
ψ=0

Fig. IV-1-1.3

can easily be seen as a velocity decrement in the velocity profiles at two inches and four inches downstream. This effect is not readily apparent in the velocity profiles further downstream. The boundary layers on the upper and lower walls of the wind tunnel have not seriously affected the velocity distribution in the mixing region even at thirteen inches downstream.

The turbulence intensity profiles for this case are shown in Figure IV-1-1.4. The profiles at one-half inch and two inches downstream exhibit the two maximum points characteristic of wake profiles. However, further downstream the profiles exhibit a single maximum, the width of the higher turbulence region increases and the maximum value of the turbulence intensity remains nearly constant.

The initial and downstream velocity profiles for the cases of $\lambda = 0.4$, 0.6 and 0.8 are shown in Figures IV-1-1.5, IV-1-1.7 and IV-1-1.9 respectively. In these figures it can be seen that the effect of the boundary layers on the separating plate becomes less evident as the velocity ratio is increased. However, while this effect cannot be seen as a large velocity decrement in the velocity profiles, at relatively short distances downstream the velocity near the center line is still lowered somewhat by this effect. From these figures, it can be seen that the width of the mixing region increases more rapidly with distance downstream as the velocity ratio is increased. Because of this, the boundary layers on the upper and lower walls of

TURBULENCE INTENSITY PROFILES HOMOGENEOUS CASE

$\lambda = 0.2$

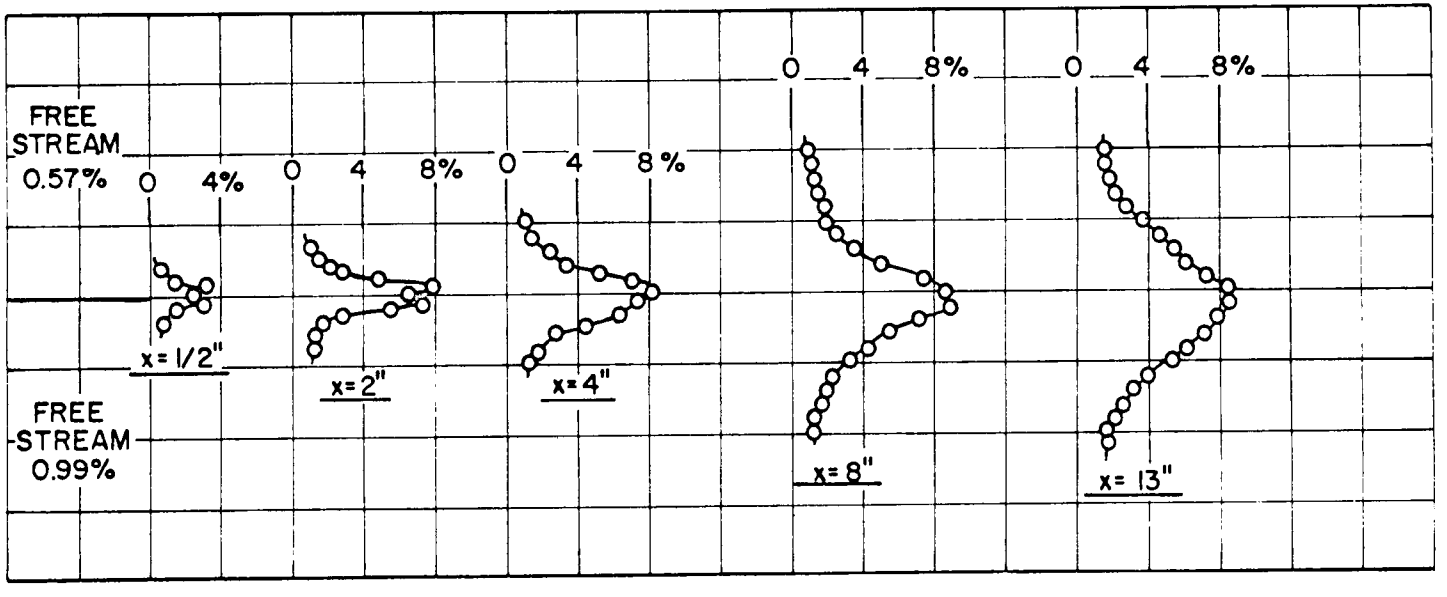

Fig. IV-1-1.4

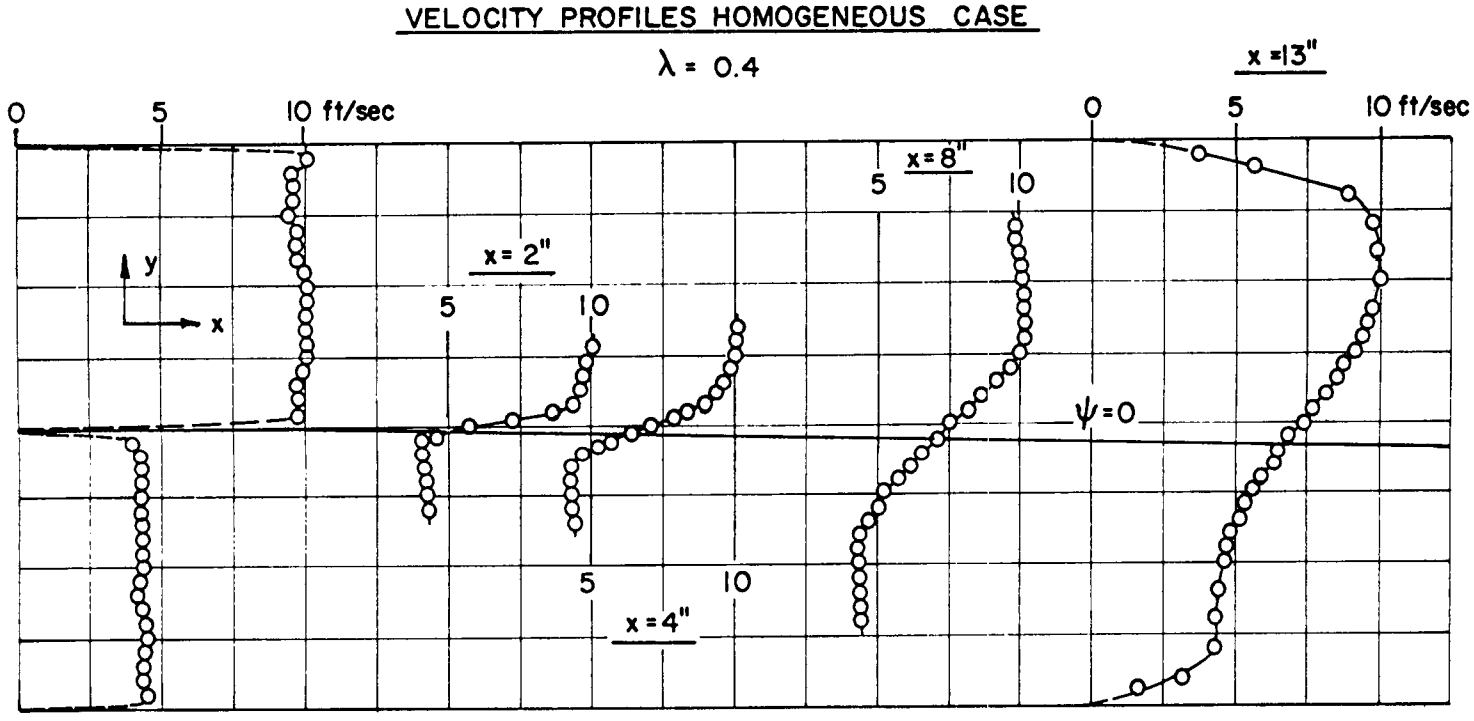
VELOCITY PROFILES HOMOGENEOUS CASE
λ = 0.4
0
5
10 ft/sec
y
x
x = 2"
x = 4"
x = 8"
x = 13"
ψ = 0

Fig. IV-1-1.5

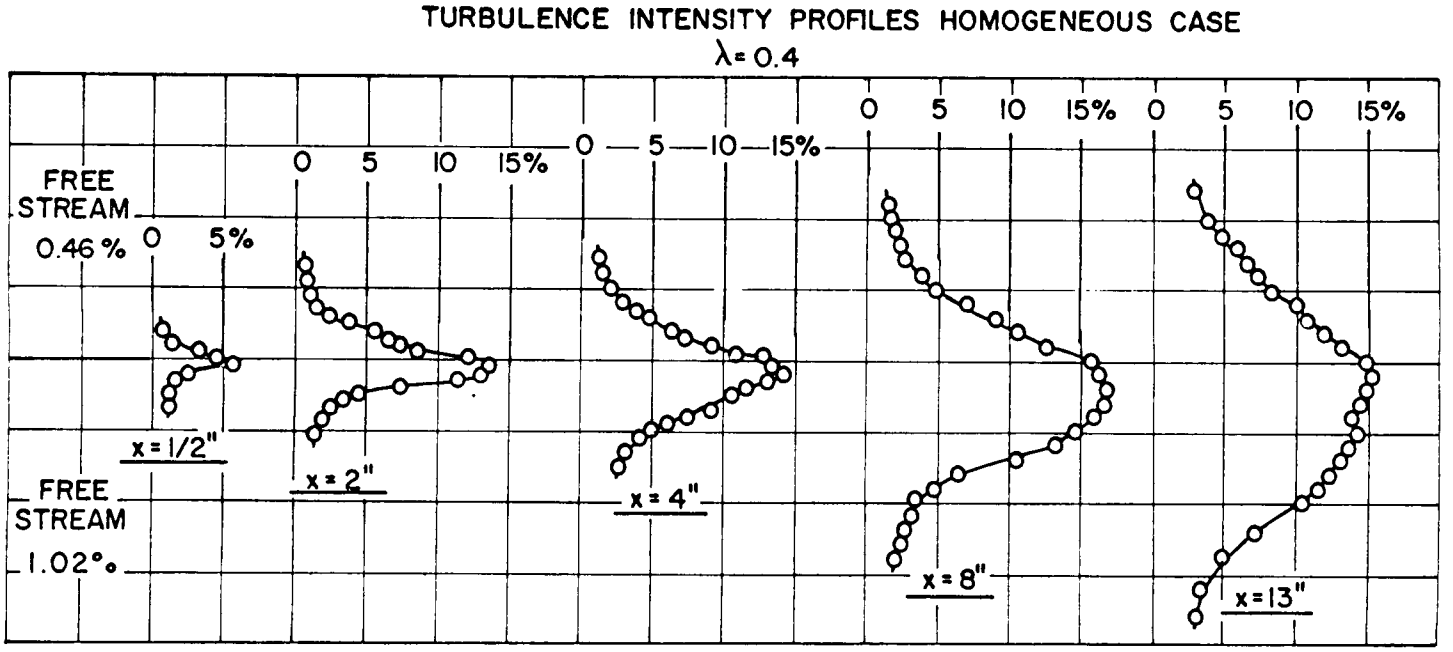
TURBULENCE INTENSITY PROFILES HOMOGENEOUS CASE
λ= 0.4
FREE STREAM 0.46 %
FREE STREAM 1.02%
0 5 10 15%
0 5%
x = 1/2"
x = 2"
x = 4"
x = 8"
x = 13"

Fig. IV-1-1.6

VELOCITY PROFILES HOMOGENEOUS CASE

$\lambda = 0.6$

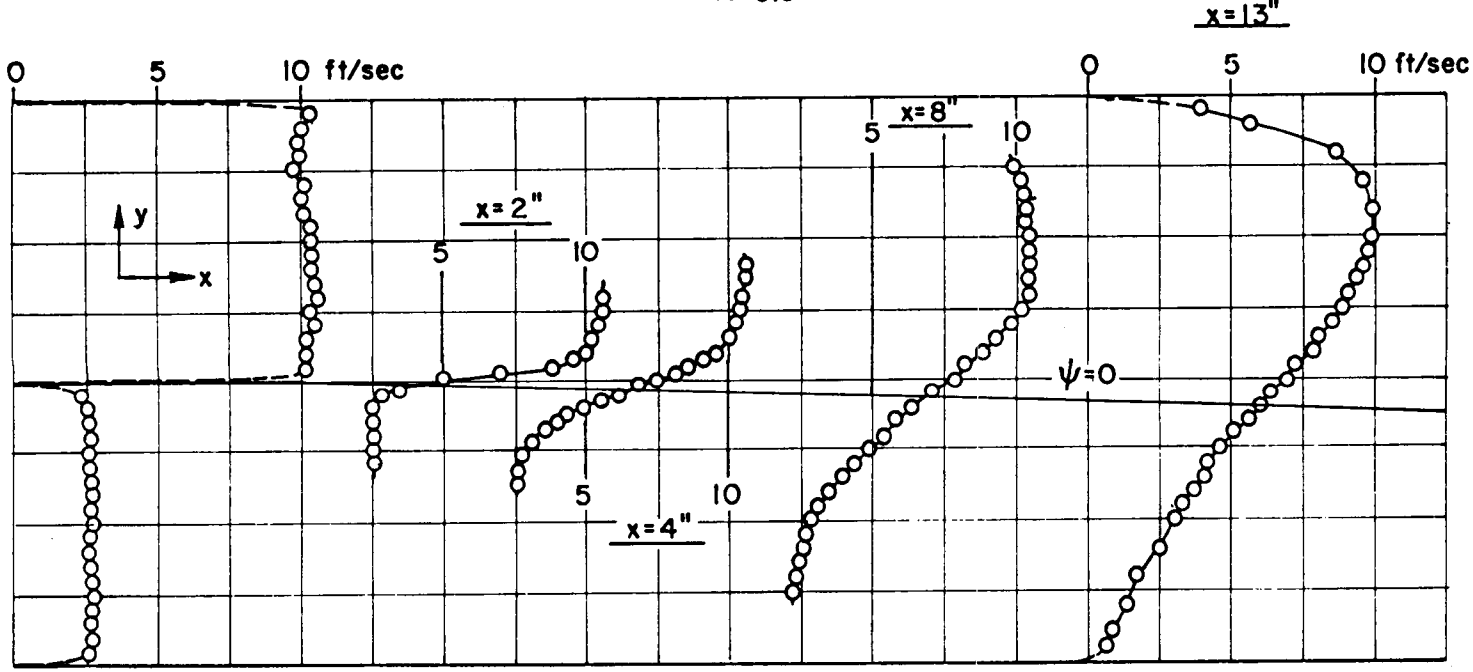

Fig. IV.-1-1.7

TURBULENCE INTENSITY PROFILES HOMOGENEOUS CASE

$\lambda = 0.6$

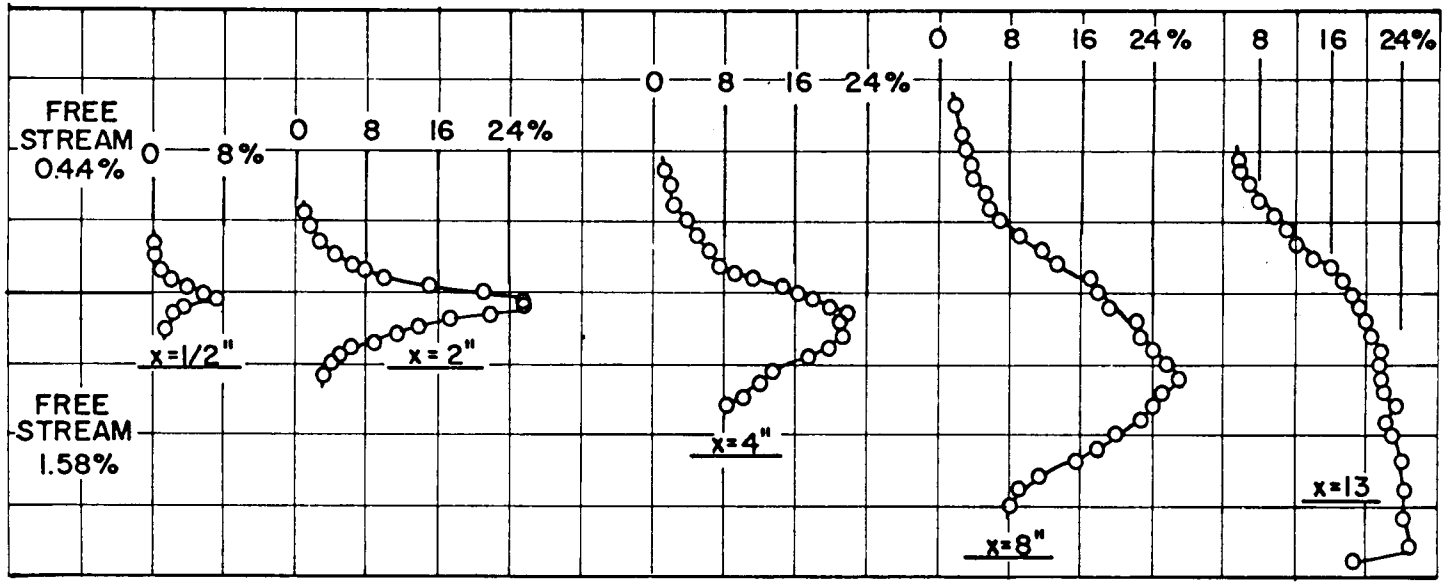

Fig. IV-1-1.8

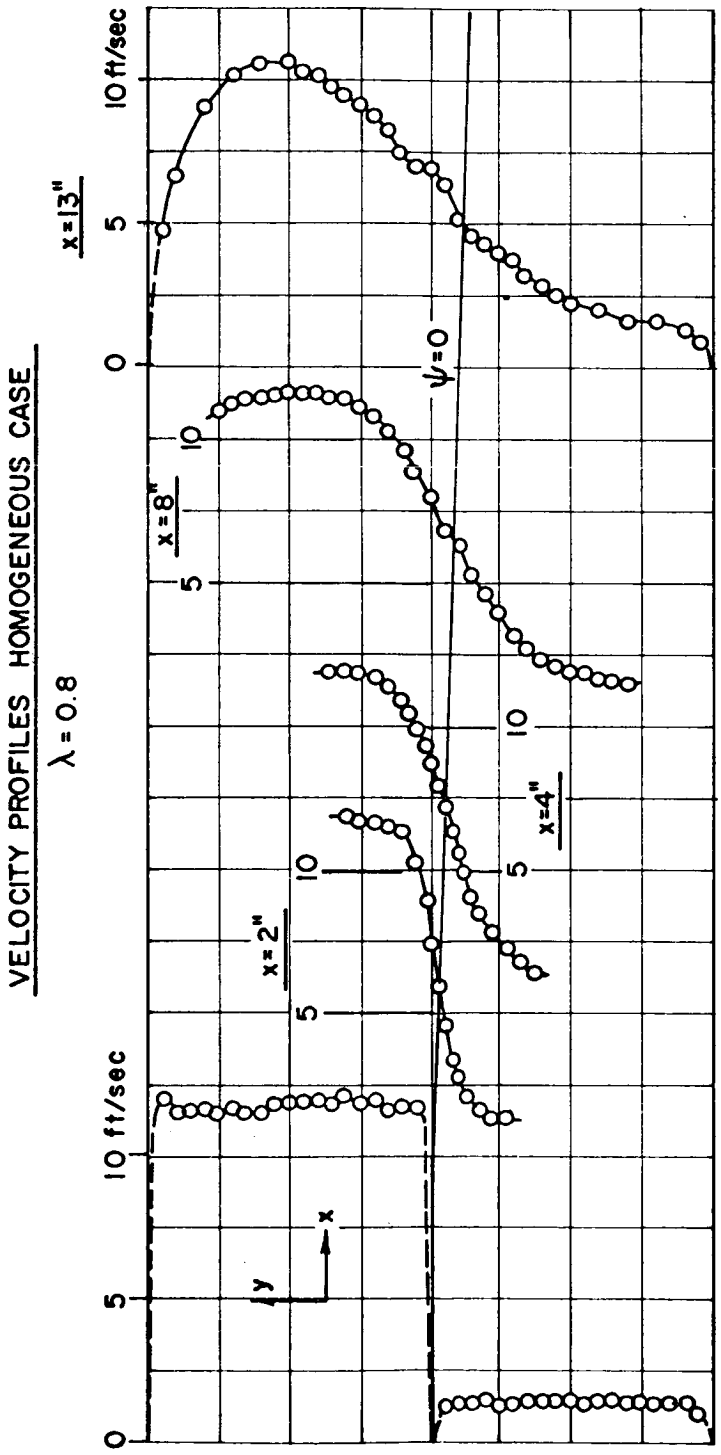
VELOCITY PROFILES HOMOGENEOUS CASE
λ = 0.8
x=13"
x=8"
x=4"
x=2"
ψ=0
10 ft/sec
0
5
10
y
x

Fig. IV-1-1.9

TURBULENCE INTENSITY PROFILES HOMOGENEOUS CASE

$\lambda = 0.8$

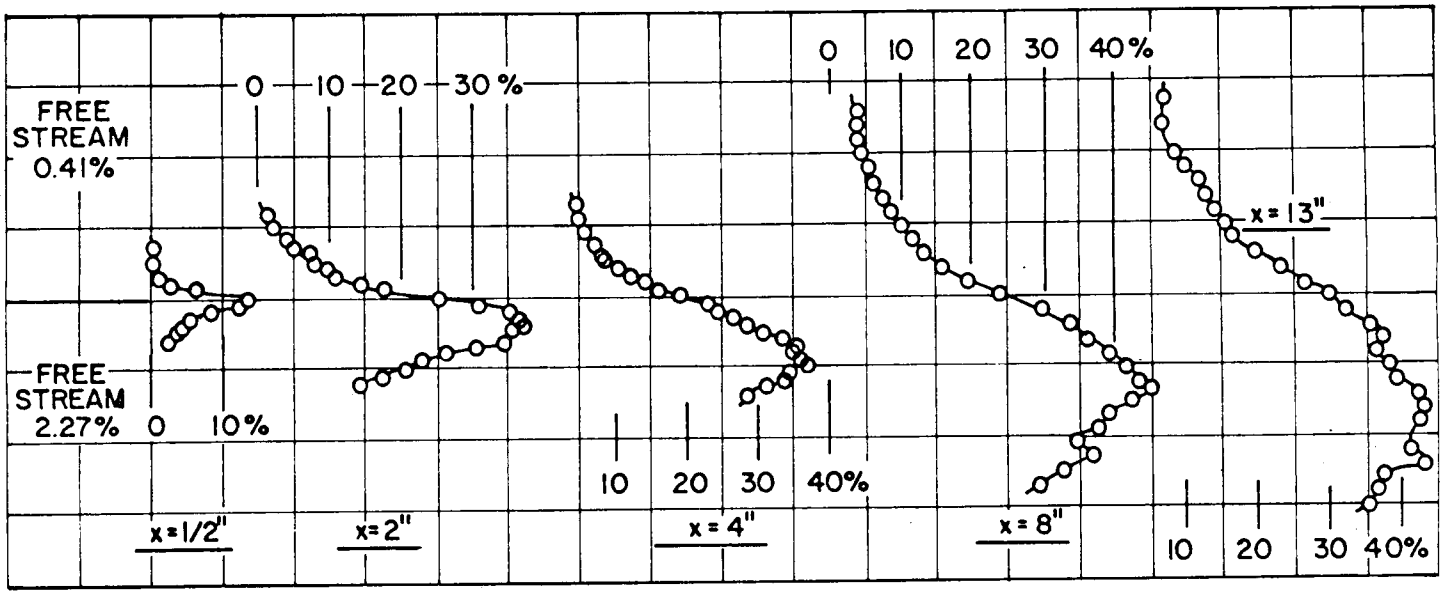

Fig. IV -1-1.10

the wind tunnel tend to interefere with the velocity profiles at larger distances downstream. This is especially evident in the profiles at x = 13" shown in Figures IV-1-1.7 and IV-1-1.9.

The turbulence intensity profiles for these cases are shown in Figures IV-1-1.6, IV-1-1.8 and IV-1-1.10. The two maximum points characteristic of wake profiles are not evident in any of these profiles. In each instance, the turbulence intensity on the center line increases rapidly from the beginning of the mixing region to a downstream distance of two to four inches and then remains approximately constant indicating that similarity of profiles should exist in this region, i.e., the similarity analysis predicts that $\overline{u'v'}$ should be constant on the centerline. As the velocity ratio is increased, the maximum value of the turbulence intensity increases and the position of this maximum shifts toward the slower moving stream. In each case the width of the higher turbulence intensity region increases with increasing distance downstream and in no case is any interference from turbulence generated near the walls of the wind tunnel apparent.

IV-1-2 Heterogeneous Case

Data are presented in this section for air mixing with Freon 12 and air mixing with freon C318. At standard conditions, freon 12 is about four times heavier than air and freon C318 is approximately seven times as dense as air. The initial turbulence intensities were again kept as

low as possible. Velocity profiles for air mixing with freon 12 at different velocity ratios are presented in Figures IV-1-2.1, IV-1-2.3 and IV-1-2.5. For the λ values of 1/3, 0.6 and 0.8, the corresponding velocity ratios are 2 to 1, 4 to 1, and 9 to 1.

For $\lambda = 1/3$ the effects of the initial boundary layers on the separating plate and the boundary layers on the walls of the wind tunnel can be easily seen. For the higher values of λ, these effects are less apparent.

The density profiles for these three velocity ratios are shown in Figures IV-1-2.2, IV-1-2.4 and IV-1-2.6. It is evident from these figures that the width of the mixing region for density also increases with increasing velocity ratio.

Turbulence intensity profiles and fluctuating density profiles were calculated using the procedure outlined in sections III-2-1 and III-2-3. However, it was found that very small changes in the calibration curves and relatively small changes in the values of the rms power readings resulted in large changes in the values of the calculated turbulence intensity and fluctuating density. Because of this, the results of the turbulence intensity and fluctuating density calculations were disregarded. A more extensive discussion of the calculation of these quantities by use of a parallel wire probe and the inherent difficulties of this method are given by Zawacki.[67]

VELOCITY PROFILES FREON-12-AIR

$\lambda = 1/3$

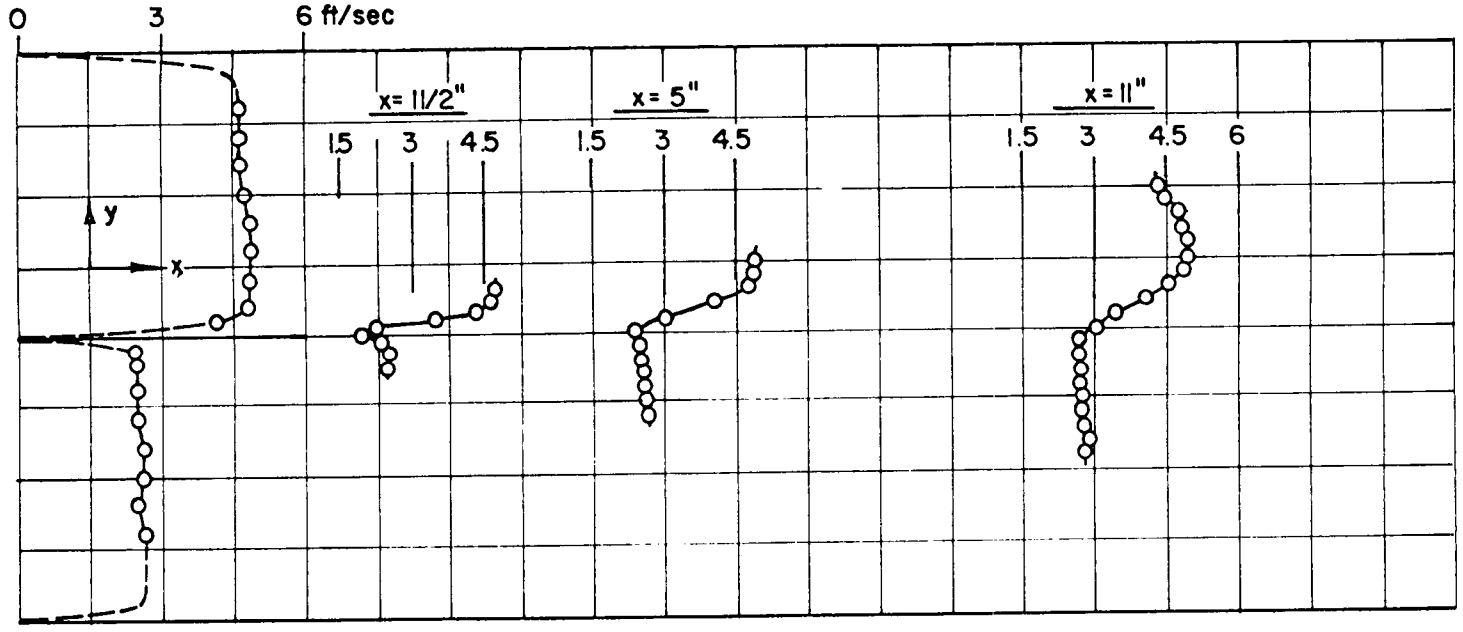

Fig. IV-1-2.1

DENSITY PROFILES FREON-12-AIR

$\lambda = 1/3$

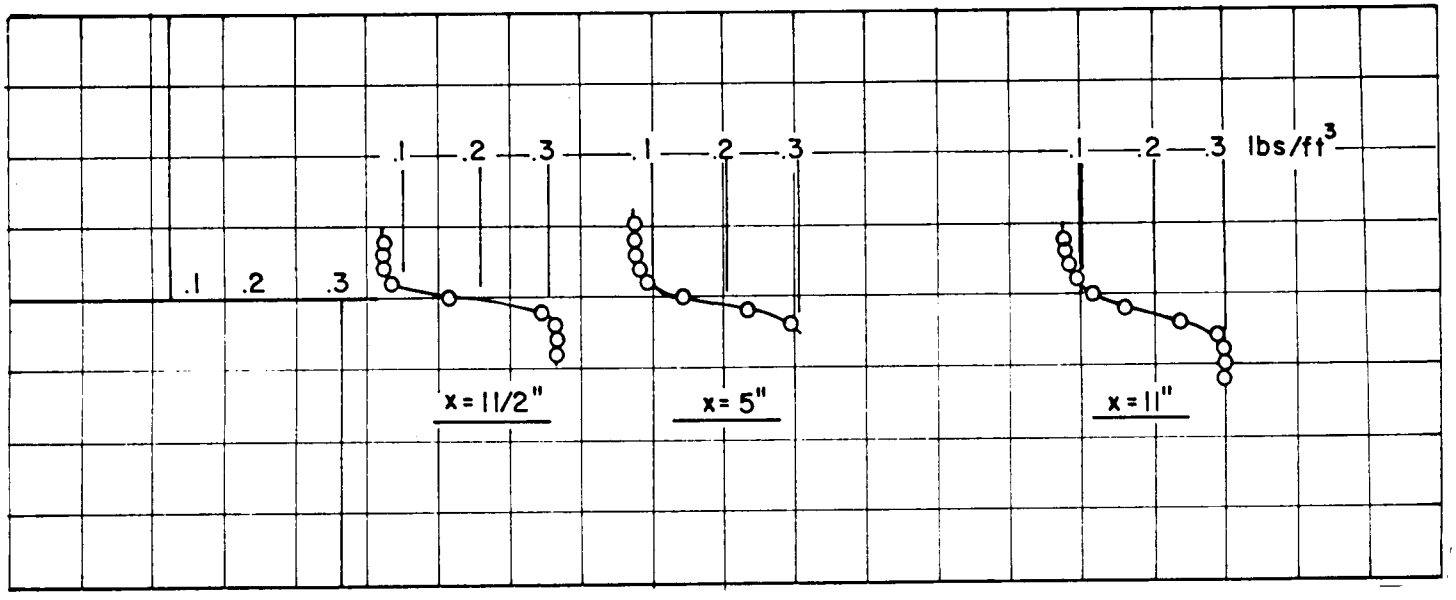

Fig. IV.-1-2.2

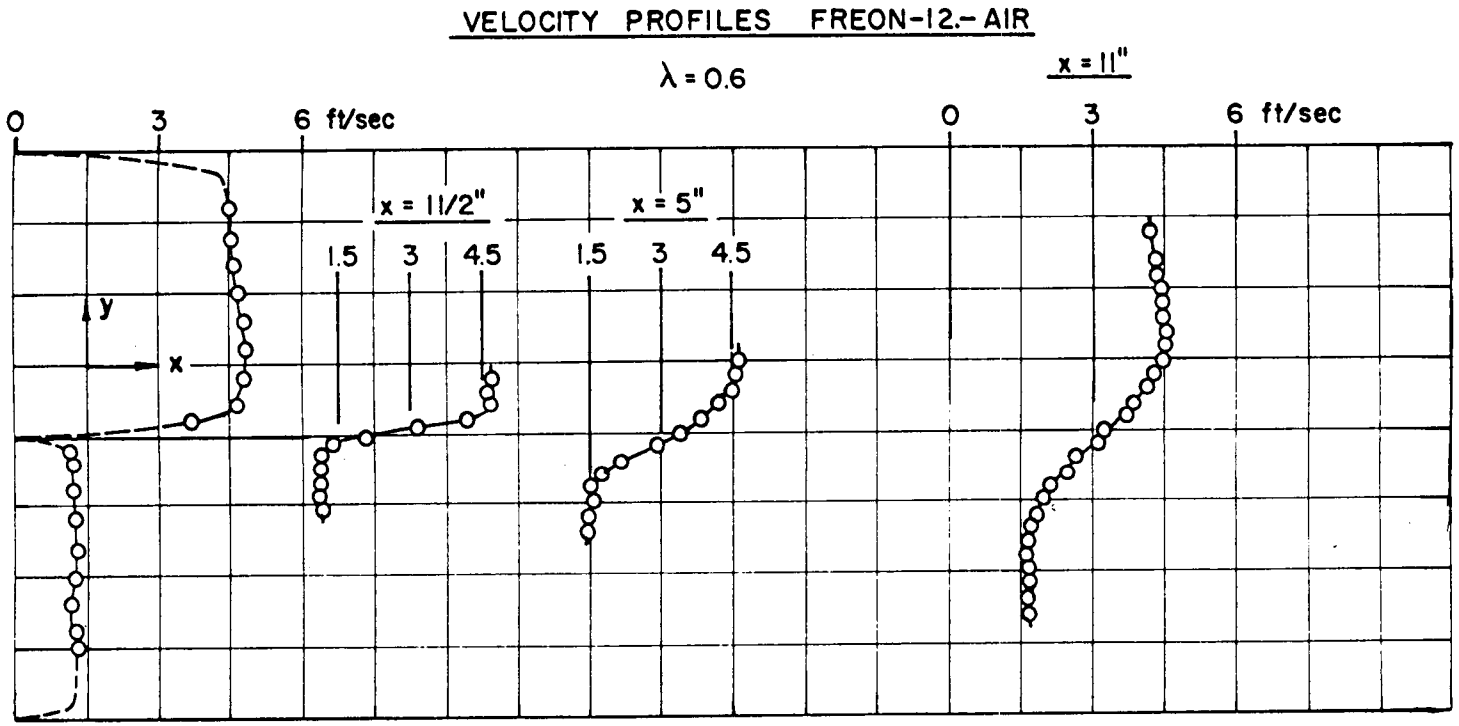
VELOCITY PROFILES FREON-12.- AIR
λ = 0.6
0
3
6 ft/sec
x = 11/2"
x = 5"
x = 11"
1.5
3
4.5
y
x

Fig. IV-1-2.3

DENSITY PROFILES FREON-12-AIR

$\lambda = 0.6$

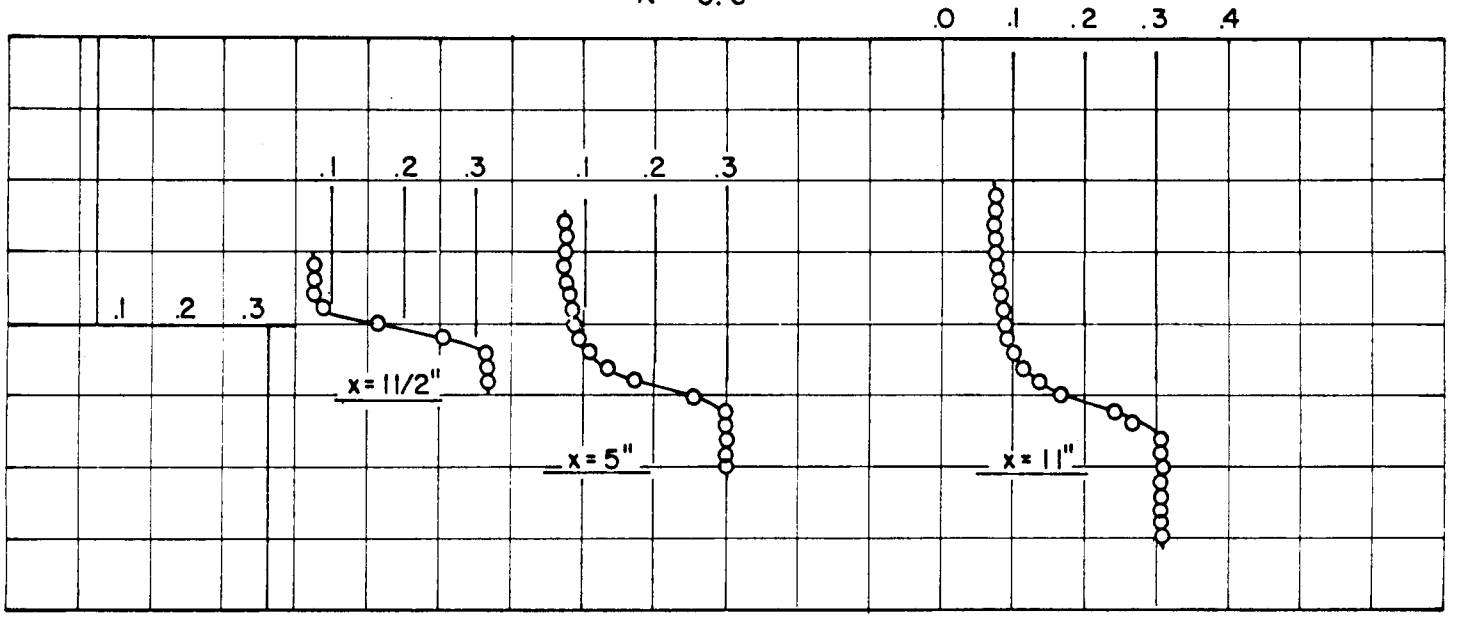

Fig. IV-1-2.4

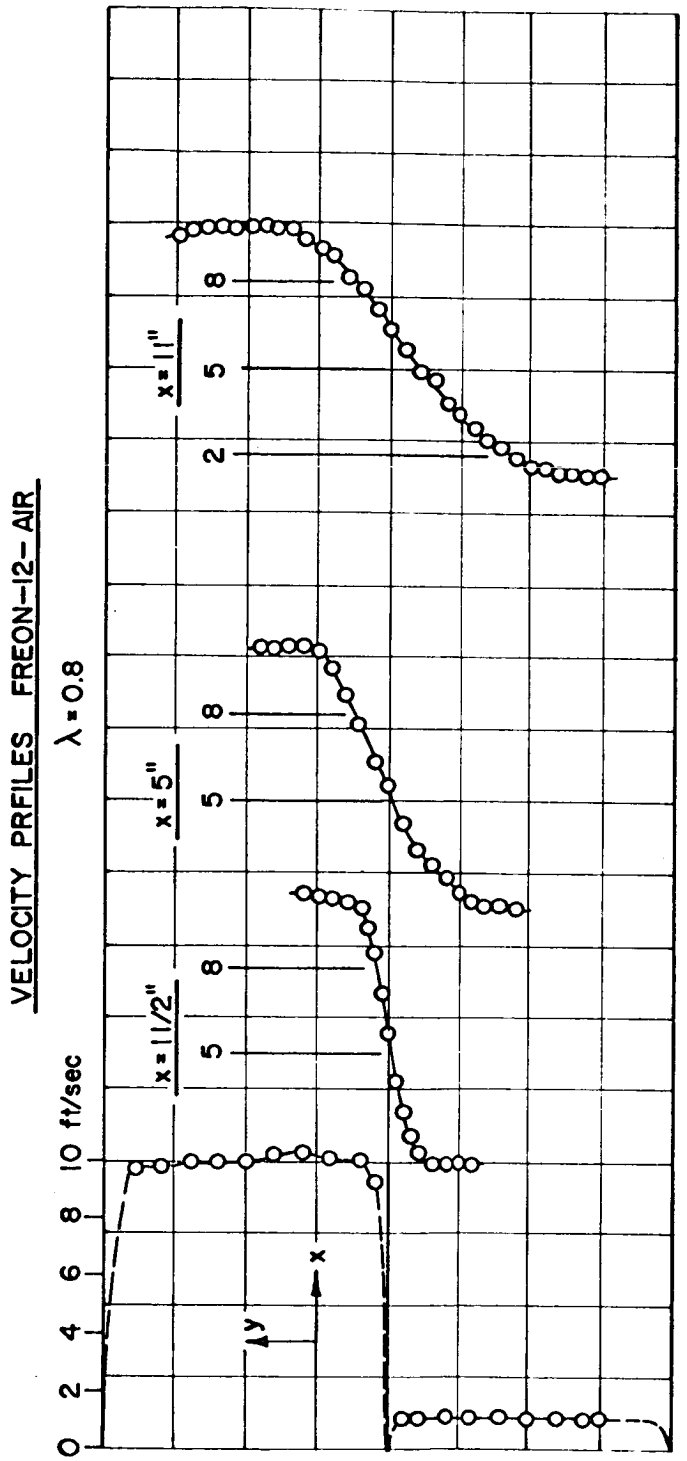
VELOCITY PRFILES FREON-12-AIR
λ = 0.8
0 2 4 6 8 10 ft/sec
x = 11/2"
x = 5"
x = 11"
5 8
5 8
2 5 8
y
x

Fig. IV-1-2.5

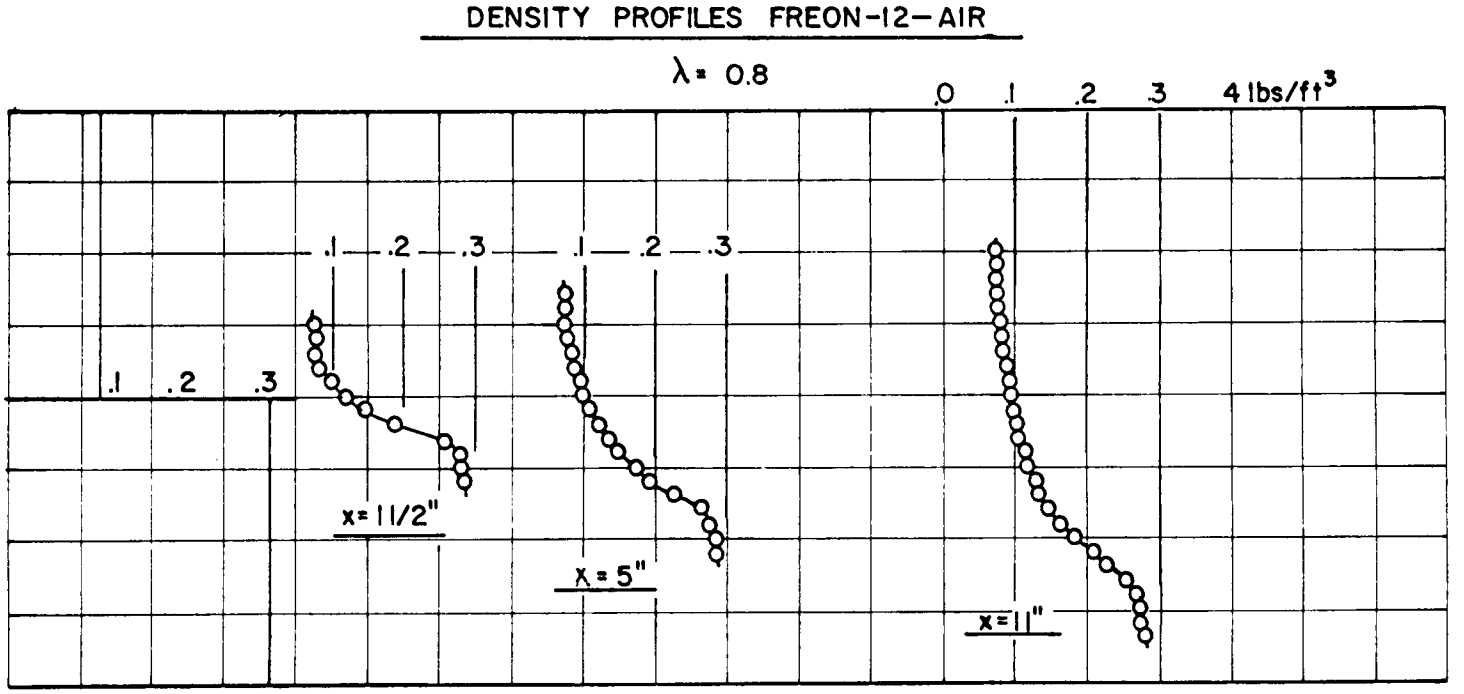
DENSITY PROFILES FREON-12—AIR
λ = 0.8
.0 .1 .2 .3 4 lbs/ft³
.1 .2 .3
.1 .2 .3
.1 .2 .3
x = 1 1/2"
X = 5"
x = 11"

Fig. IV-1-2.6

Velocity profiles for air mixing with freon C318 at a velocity ratio of 7 to 1 are shown in Figure IV-1-2.7. The corresponding value of λ is 0.75. The density profiles for this case are shown in Figure IV-1-2.8. The velocity profiles do not appear to be affected by the boundary layers on the walls of the wind tunnel. The density profiles indicate a very gradual increase in the density coming down through the mixing region and then a very steep density gradient near the lower edge of the mixing region. This is probably caused by a retarding of the upward movement of the higher density gas by the gravitational body force. The turbulence intensity and fluctuating density profiles were calculated for this case. However, because of the inaccuracies discussed above in connection with freon 12-air data, the results of these calculations were also disregarded.

IV-2 Similarity

Since laminar mixing was not observed experimentally, the discussion here will be concerned with comparing the experimental data with the turbulent homogeneous and heterogeneous similarity solutions obtained in Ref. 67. The good agreement of the experimental data with the turbulent similarity solution indicates that the laminar similarity solution should be a good representation of the laminar velocity profiles.

VELOCITY PROFILES FREON C 318-AIR

$\lambda = 0.75$

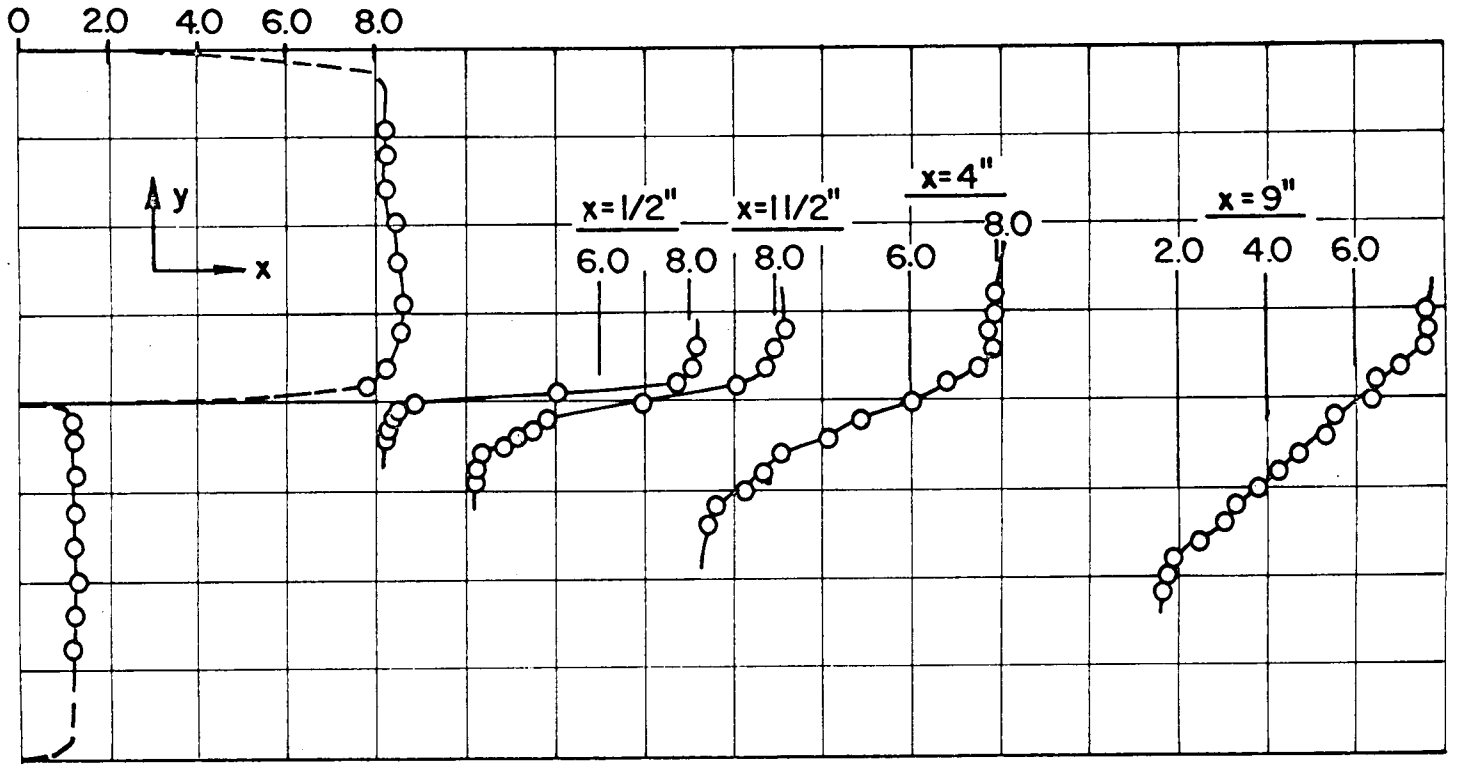

Fig. IV-1-2.7

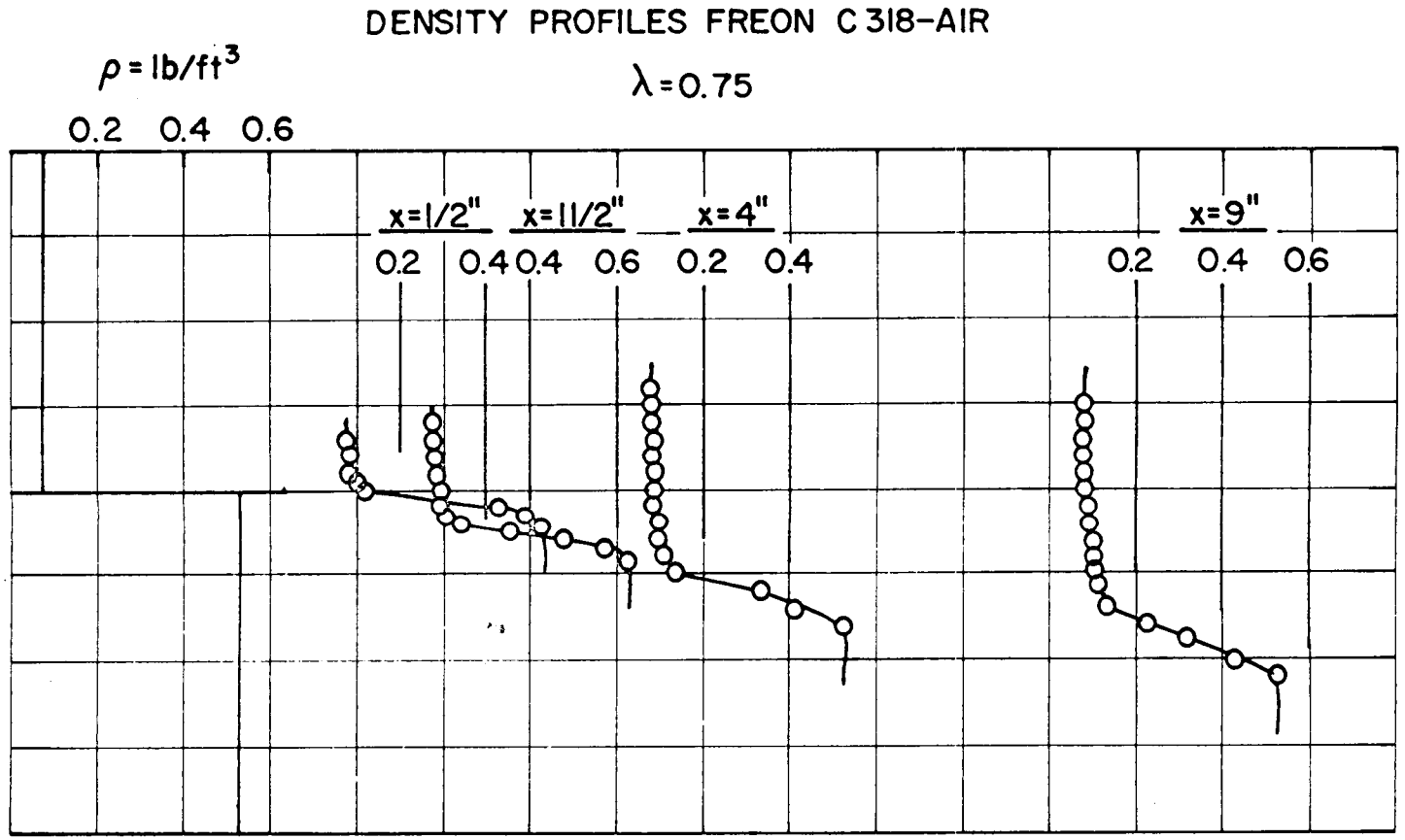
DENSITY PROFILES FREON C 318-AIR
ρ = lb/ft³
λ = 0.75
0.2 0.4 0.6
x=1/2"
x=11/2"
x=4"
x=9"
0.2 0.4 0.4 0.6 0.2 0.4
0.2 0.4 0.6

Fig. IV -1-2.8

IV-2-1 Homogeneous Case

Before comparing the homogeneous turbulent similarity solution with the experimental data presented in section IV-1-1, it is interesting to compare this solution with previous experimental data. The best previously available data is that given by Liepmann and Laufer[12] and by Albertson.[14]

Liepmann and Laufer compared their measurements with the theoretical solution of Goertler, (See reference 67 and section II-1). However, Goertler applied an arbitrary third boundary condition. (See reference 67). Therefore, it was necessary for Liepmann and Laufer to obtain the location of the line $\xi^* = 0$ in the x-y plane from their experimental data, i.e., for a particular value of x, that point in the velocity profile for which $u = \frac{1}{2}(u_1 + u_2)$ was designated $y^* = 0$ or $\xi^* = \sigma \frac{y^*}{x} = 0$ in accordance with the arbitrary third boundary condition

$$F'(6) = \frac{u}{U} = 1$$

or

$$u = \frac{1}{2}(u_1 + u_2)$$

The application of the third boundary condition suggested by von Karman, as outlined in reference 67 makes it unnecessary to locate the position of an arbitrary line in the x-y plane from experimental data. Rather, the line $\xi = 0$ is the x-axis ($y = 0$) and the line $\xi^* = 0$ or $\xi = \sigma \frac{y}{x} = \xi_o$ is the $\psi = 0$ streamline in the x-y plane.

From the data of Liepmann and Laufer, the constants σ, c and x, which appear in the homogeneous similarity solution may be easily calculated using the procedure outlined in reference 67. The calculated values of these constants are:

From the data of Liepmann and Laufer	$\sigma = 12.49$ $c = 0.207$ $\chi_1 = 0.00775$	IV-2-1.1

Liepmann and Laufer's experimental data and the similarity solution employing von Karman's third boundary condition are compared in Figure IV-2-1.1. The measurements agree quite well with the theoretical curve.

Albertson demonstrated that the velocity profiles in the initial mixing region of his slot-jet were similar in y/x. However, he did not attempt to compare his data with a similar solution of the equations of continuity and momentum. Rather, he presented a two parameter empirical relationship which approximated the data reasonably well. (See section II -1).

From the experimental data of Albertson, the calculated values of σ, c and χ_1 are:

From the data of Albertson[14]	$\sigma = 13.38$ $c = 0.194$ $\chi_1 = 0.00719$	IV-2-1.2

Albertson's measurements and the similarity solution employing von Karman's third boundary condition are compared in Figure IV -2-1.2. The data agrees reasonably well with the theoretical curve at higher velocities, but rather large

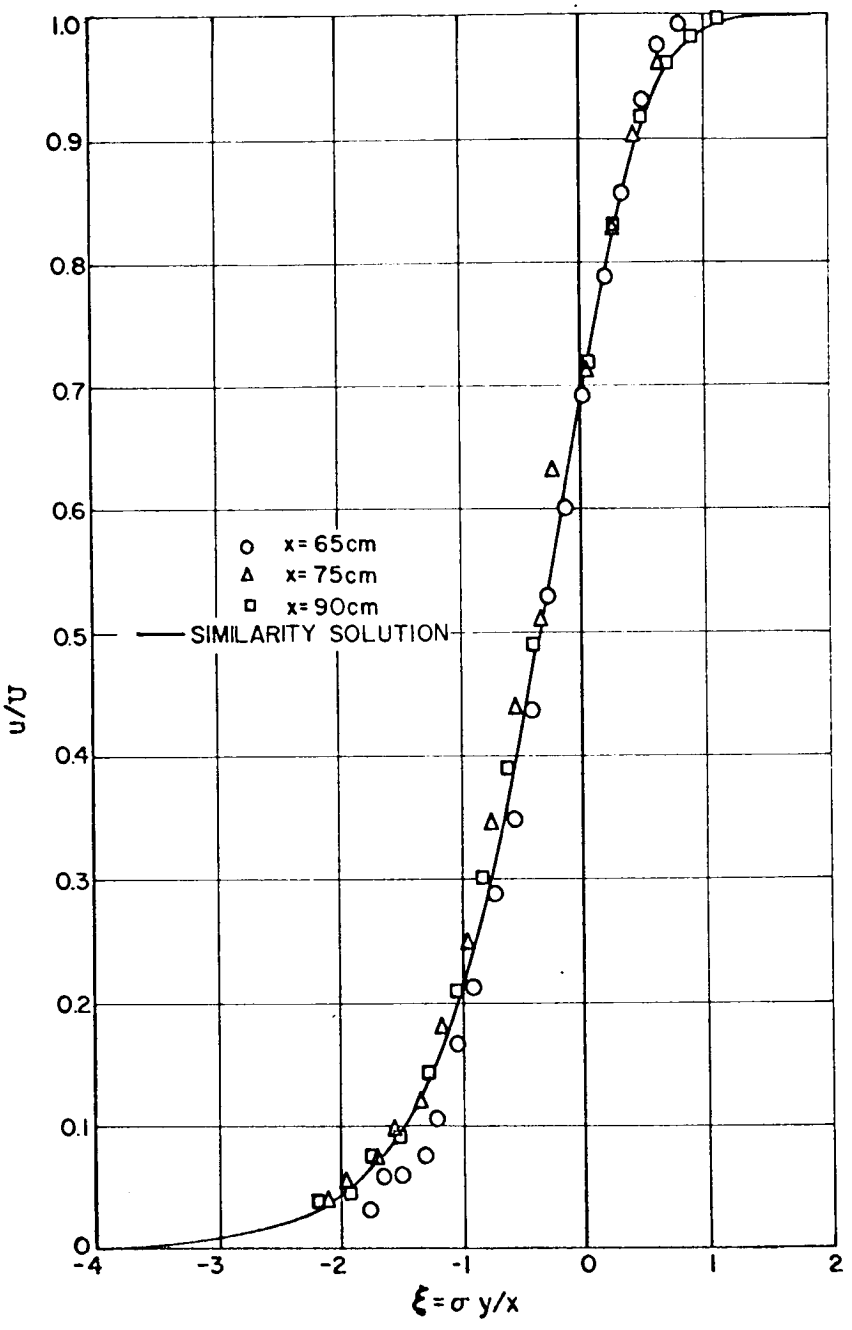

Fig. IV-2-1.1 Comparison of Similarity Solution Data of Liepmann and Laufer[36]

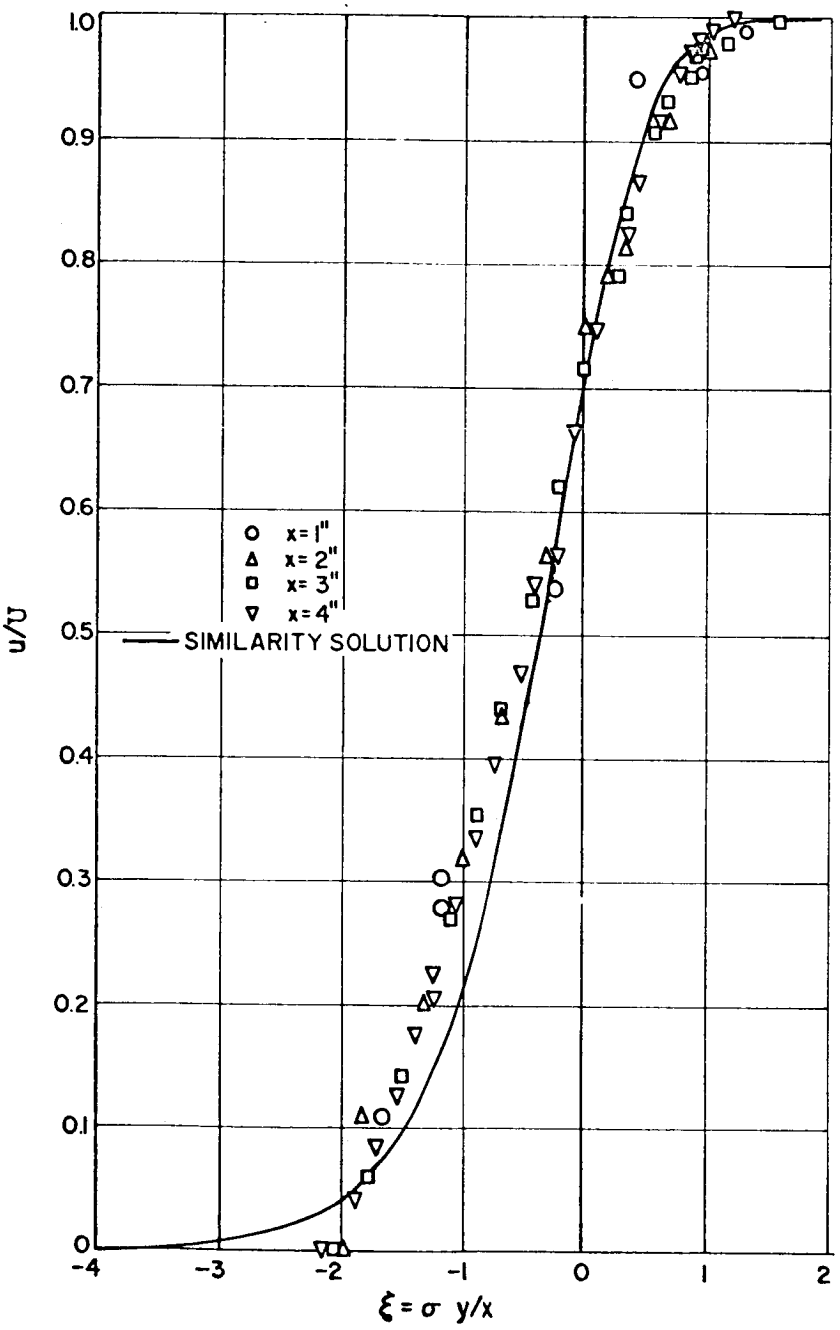

Fig. IV-2-1.2 Comparison of Similarity Solution with the Data of Albertson[35]

deviations occur at lower velocities. This is most likely because the initial mixing region of a slot-jet is not wholely comparable to a true half-jet.

In section IV-1-1, two factors, in addition to the velocity ratio, were discussed which affect the velocity profiles in the mixing region. These factors were the boundary layers on the plate initially separating the two streams and the boundary layers which build up on the upper and lower walls of the wind tunnel. From the figures presented in section IV-1-1, it can be easily seen that the effect of the first factor is most evident in the initial part of the mixing region, whereas the effect of the second factor is evident at large distances downstream. In between these two regions, $\overline{u'^2}$ is constant on the center-line and the velocity profiles should be nearly similar.

Experimental data from section IV -1-1 is compared with the similarity solution for various values of λ in Figure IV -2-1.3. The measurements, in a region where the effects of the above mentioned factors are minimized, agree reasonably well with the theoretical curves. The calculated values of the constants σ, c and χ_1 and eddy viscosity ϵ for various values of λ are summarized in Table IV-2-1.1.

Two significant facts are evident from examining Table IV -2-1.1. First, the constant c expressing the rate of linear growth of the width of the mixing region with downstream distance χ increases monotonically with increasing λ. Second, the eddy viscosity ϵ is proportional

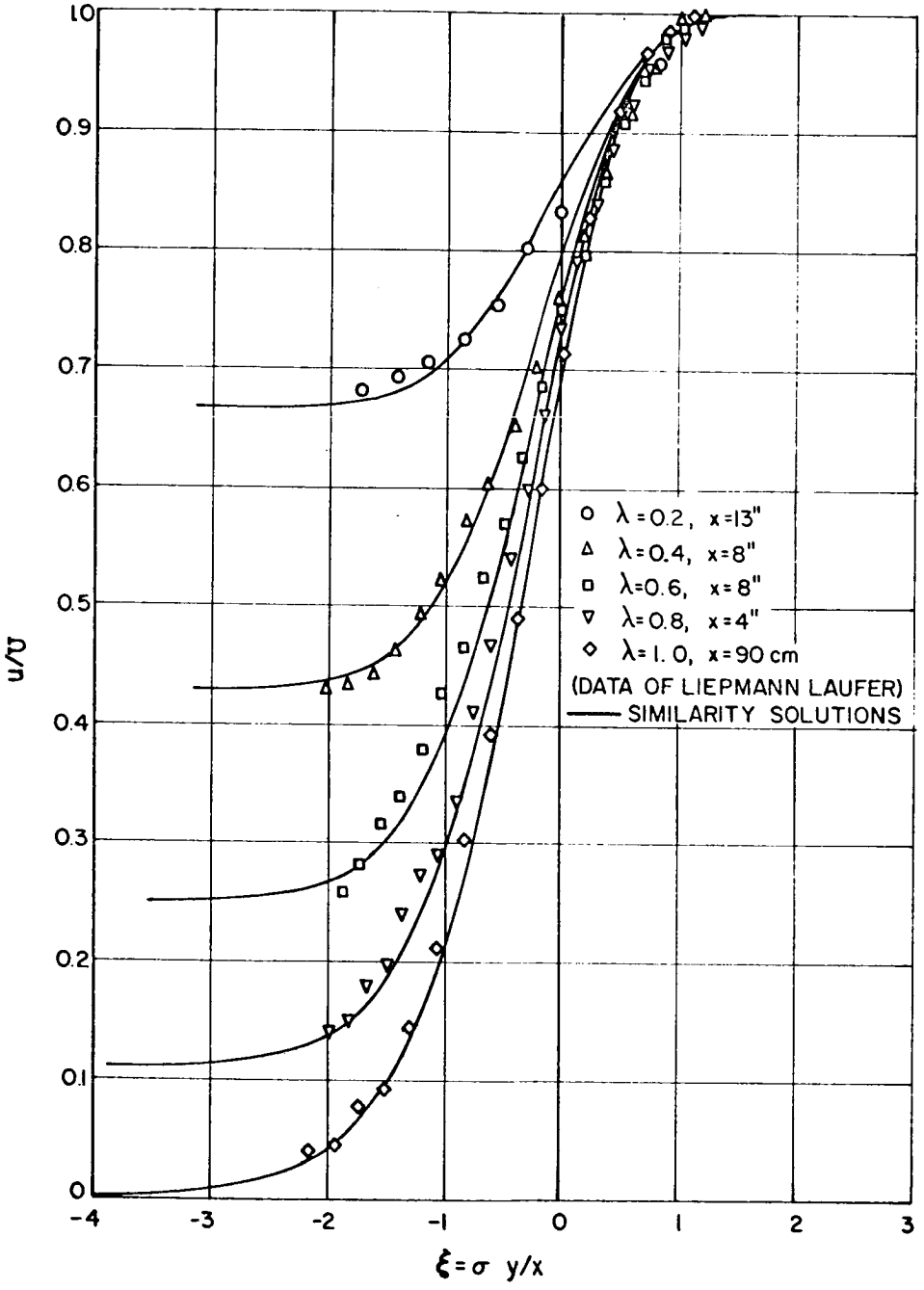

Fig. IV-2-1.3 Similarity Solution and Data For Various Values of λ

Table IV-2-1.1 Summary of Calculated Constants

	σ	c	χ_1	$\epsilon = \chi_1 \, c \, x \, (u_1 - u_2)$
$\lambda = 0.2$	37.5	0.0615	0.0145	$0.000892 \, x \, (u_1 - u_2)$
$\lambda = 0.4$	16.01	0.146	0.0167	$0.00244 \, x \, (u_1 - u_2)$
$\lambda = 0.6$	13.75	0.173	0.0127	$0.00219 \, x \, (u_1 - u_2)$
$\lambda = 0.8$	12.10	0.205	0.0104	$0.00213 \, x \, (u_1 - u_2)$
$\lambda = 1.0$ (Liepmann and Laufer)	12.49	0.207	0.00225	$0.00165 \, x \, (u_1 - u_2)$
$\lambda = 1.0$ (albertson)	13.38	0.194	0.00769	$0.00139 \, x \, (u_1 - u_2)$

to the difference in the two free stream velocities and the distance downstream and the constant of proportionality is roughly constant for all λ values ranging from 0.4 to 1.0.

In addition to supplying the theoretical u-velocity profiles for various values of λ, the similarity solution with von Karman's third boundary condition provides the theoretical v-velocity profiles and a means of locating the $\psi = 0$ streamline in the x-y plane.

In this homogeneous case, it can easily be shown that the $\psi = 0$ streamline coincides with the locus of the inflection points of the velocity profiles in the x-y plane. Since along the streamline $\psi = 0$, $\xi^* = 0$, then

$$\xi = \xi_o = \sigma \frac{Y}{x}$$

or

$$y = \frac{\xi_o}{\sigma} x = mx$$

After determining the value of ξ_o from the similarity solution and the value of σ from experimental data, the $\psi = 0$ streamline may be located in the x-y plane. The theoretical $\psi = 0$ streamlines for various values of λ are shown on the figures in section IV-1-1.

The theoretical v-velocity profiles are shown in Figure IV-2-1.4. The asymptotic values of these velocity profiles may not be correctly determined unless von Karman's third boundary condition is used or the location of the line $\xi^* = 0$ in the x-y plane is determined experimentally. Liepmann and Laufer presented the curve for $\lambda = 1.0$ after locating the line $\xi^* = 0$ from their experimental data. The curves for the other values of λ have not been previously given. It is interesting to note that the asymptotic value of v for large negative values of ξ increases monotonically with increasing λ. However, the asymptotic value of v for large positive values of ξ decreases for λ ranging from 0.2 to 0.6 but then increases when λ is increased to 0.8 and 1.0. Physically, the condition imposing the asymptotic values of the v-velocity is that given by von Karman, i.e., there is to be no net force acting on the total fluid system perpendicular to the main flow or

$$u_1 v_1 = u_2 v_2 = 0$$

Thus, since for $\lambda = 1.0$, $u_2 = 0$, then v_1 must be zero also

or the asymptotic value of v for $\lambda = 1.0$ and large positive ξ is zero.

Each v-velocity profile in Figure IV-2-1.4 exhibits a minimum point at $\xi = 0$. Thus, $\frac{\partial \xi}{\partial \eta} = 0$ for $\xi = 0$ or for a given value of x, $\frac{\partial v}{\partial y} = 0$ for $y = 0$. This shows that the v-velocity profile at a given value of x has a minimum point on the x-axis ($y = 0$). Further, from the continuity equation $\frac{\partial u}{\partial x} = 0$ or u is constant along the x-axis. Also, since $\frac{\partial v}{\partial \xi}$ is positive for plus ξ and negative for minus ξ, it follows that $\frac{\partial u}{\partial x}$ is negative for plus ξ and positive for minue ξ. In summation, the velocity along the x-axis is constant. The flow above the x-axis is decelerated while the flow below the x-axis is accelerated.

IV-2-2 Heterogeneous Case

Just as in the homogeneous case, there is a portion of the mixing region in the figure shown in section IV-1-2 where the effects of the boundary layers on the separating plate and the walls of the wind tunnel are minimized. In this section, the similarity solutions for the velocity and density profiles in the mixing region are presented. For each value of λ, the theoretical u-velocity and density profiles are given in separate figures. On each figure, the theroetical curves for Schmidt numbers of 0.5, 0.75 and 1.0 are shown.

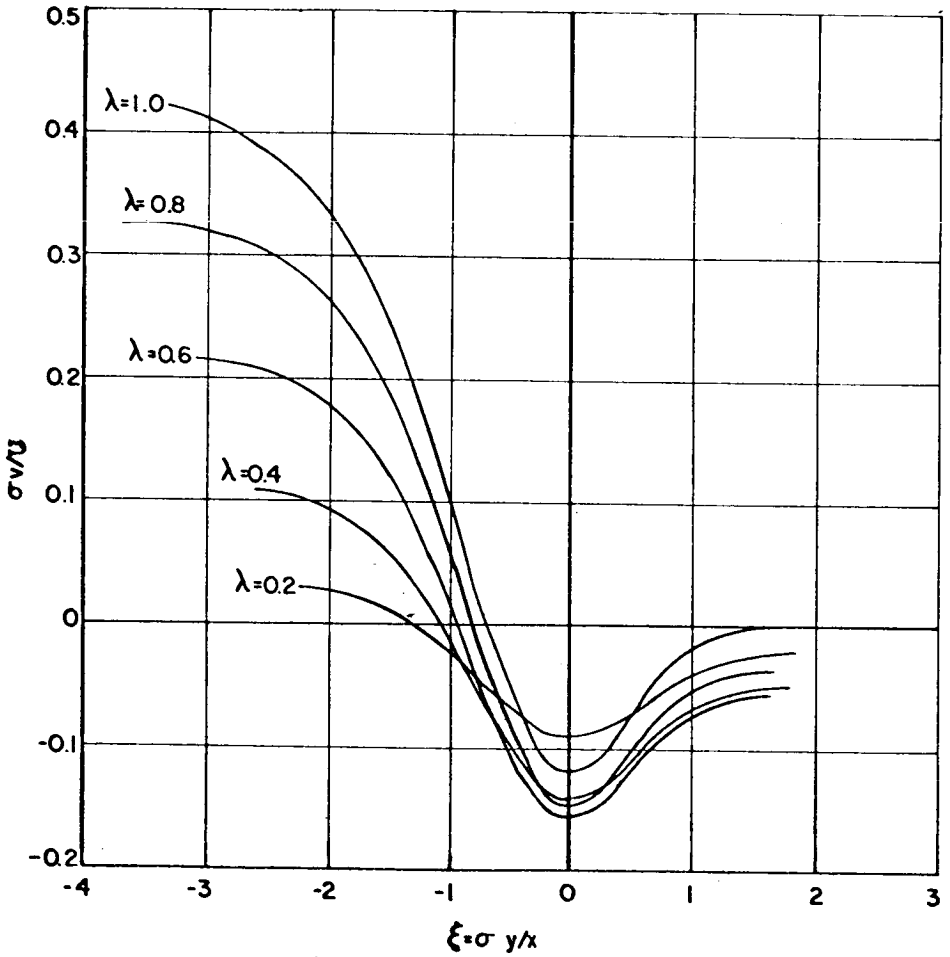

Fig. IV-2-1.4 Theoretical Transverse Velocity Profiles for The Homogeneous Case

The theoretical velocity profiles for freon 12 and air at λ values of 1/3, 0.6 and 0.8 are given in Figures IV-2-2.1, IV-2-2.2 and IV-2-2.3. Since freon 12 is about four times heavier than air, $\Gamma = -0.6$, i.e.,

$$\Gamma = \frac{\rho_1 - \rho_2}{\rho_1 + \rho_2} = -0.6$$

It follows that $\lambda = 0.6$ is the case for which the momentum of the upper and lower streams is the same.

In each figure, experimental data obtained at two downstream positions is shown. The effect of the boundary layers on the separating plate is especially evident in Figure IV-2-2.1 for $\lambda = 1/3$. For $\lambda = 0.6$ and $\lambda = 0.8$, the measurements agree reasonably well with the theoretical curves for a turbulent Schmidt number of 0.75. Theoretically, a decreasing turbulent Schmidt number displaces the u-velocity and density profiles toward the slower moving higher density stream. This follows since a decreasing Schmidt number means relatively less momentum transfer and relatively more mass transfer.

From this data, the calculated values of the constants σ, c and χ_1, for $\Gamma = -0.6$ and various values of λ are

$\Gamma = -0.6$, $\lambda = 1/3$ $\sigma = 36.9$ $c = 0.0485$, $\chi_1 = 0.0114$

$\Gamma = -0.6$, $\lambda = 0.6$ $\sigma = 15.4$ $c = 0.142$, $\chi_1 = 0.0124$

$\Gamma = -0.6$, $\lambda = 0.8$ $\sigma = 14.6$ $c = 0.181$, $\chi_1 = 0.00810$

Because of the large effect of the boundary layers on the separating plate, evident in Figures IV-1-2.1 and IV-2-2.1, the reliability of the values given for $\lambda = 1/3$ is questionable.

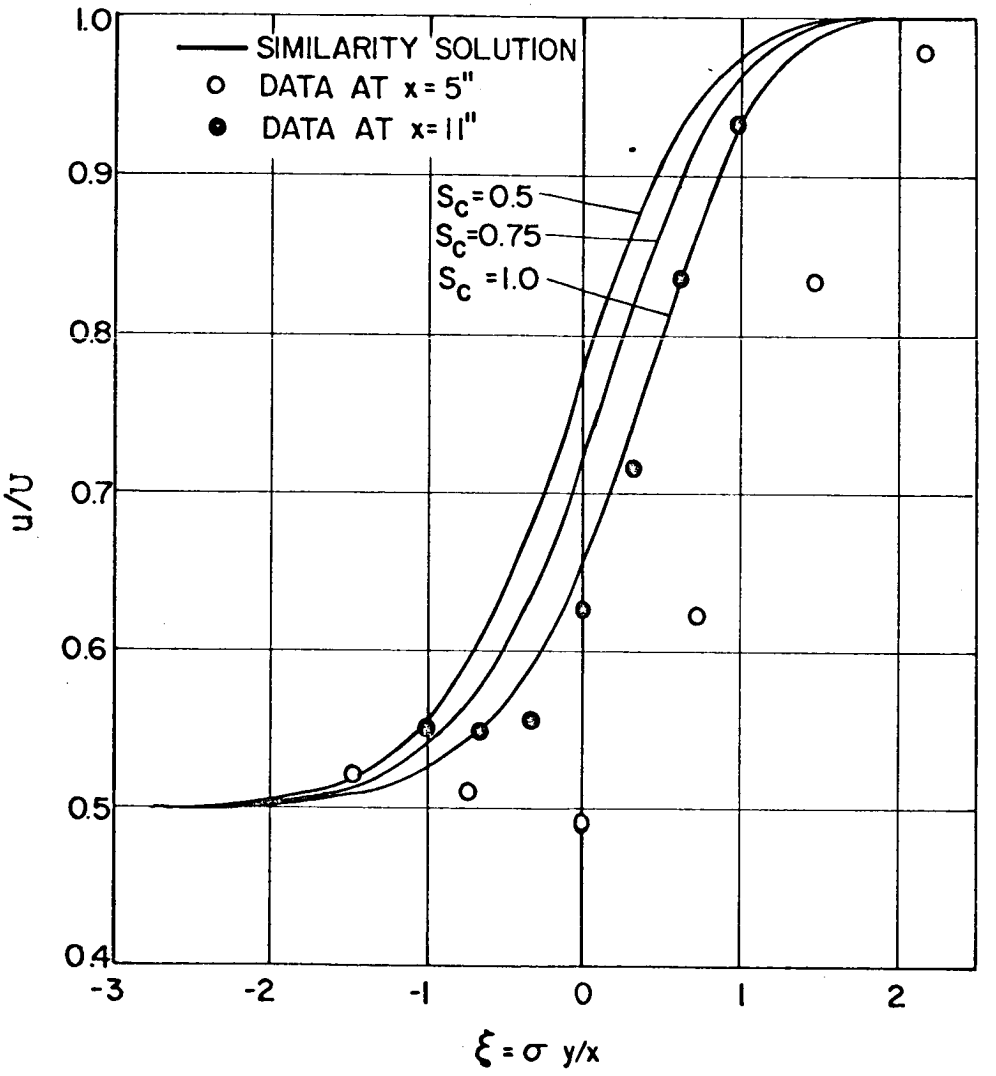

Fig. IV-2-2.1 Velocity Profiles of Freon 12-Air
λ = 1/3

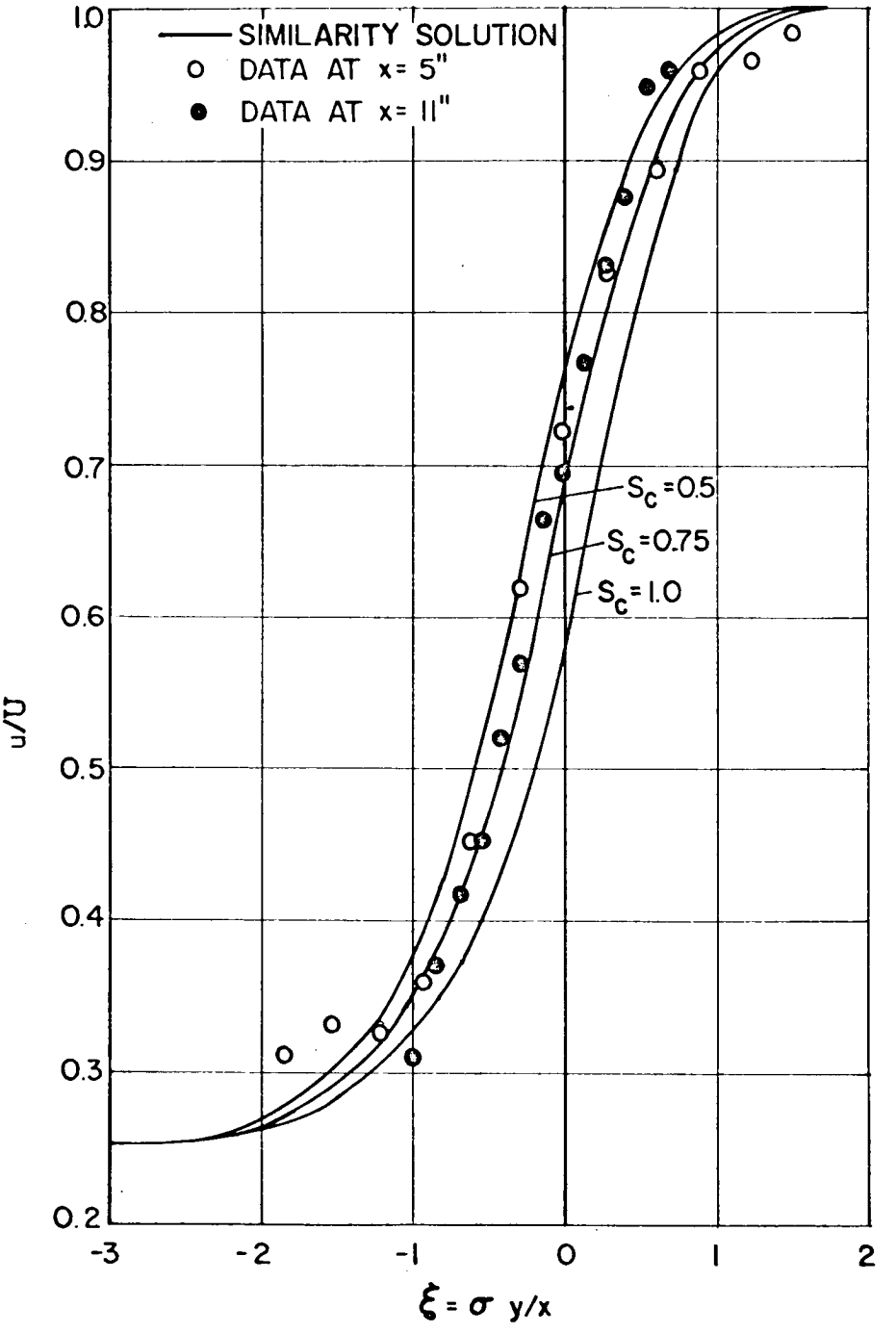

Fig. IV-2-2.2 Velocity Profiles of Freon 12-Air
λ = 0.6

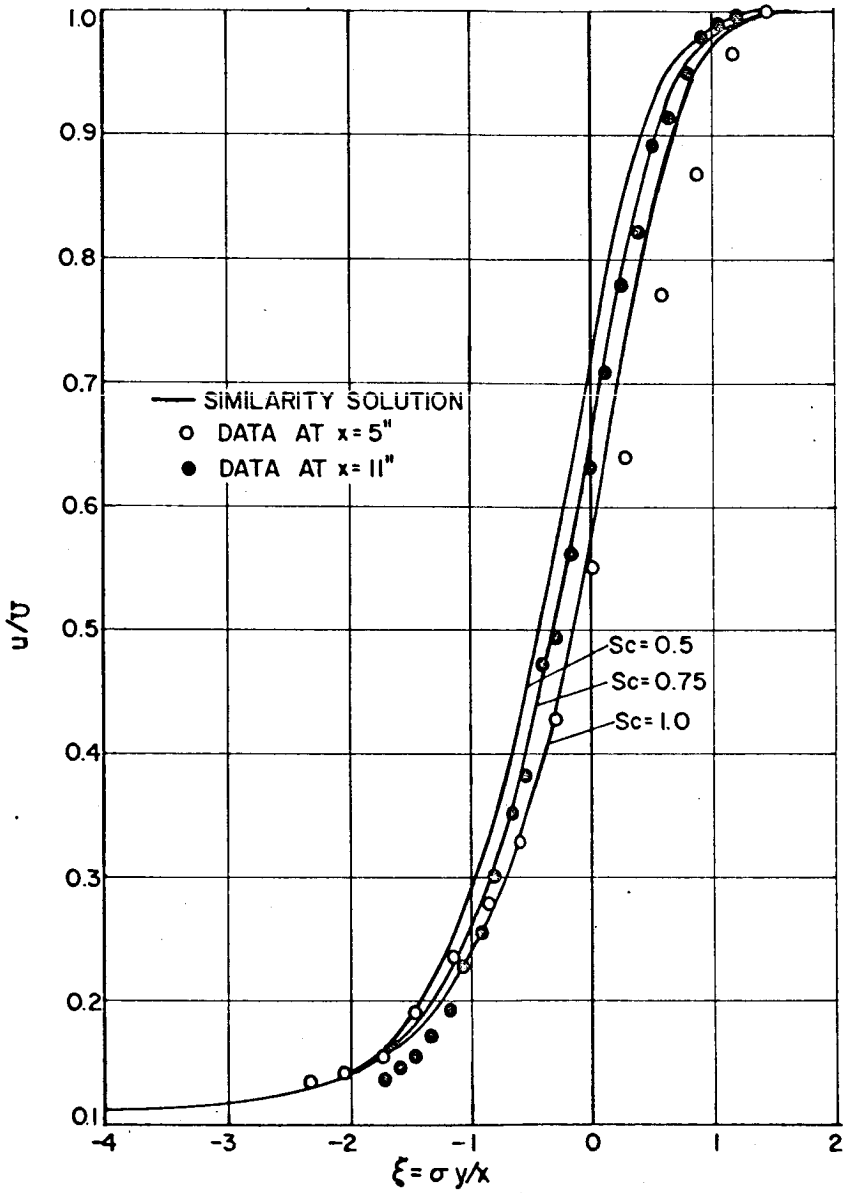

Fig. IV-2-2.3 Velocity Profiles of Freon 12-Air

$\lambda = 0.8$

The theoretical density profiles and the experimental data are compared in Figures IV-2-2.4, IV-2-2.5 and IV-2-2.6. It appears that the body force, which was neglected in the analytical analysis, has affected the experimental density profiles. Due to the body force, relatively less of the higher density gas is transported upward resulting in experimental densities higher than predicted theoretically at large negative values of ξ and experimental densities lower than those predicted by theory for larger values of ξ. Because of this, the width of the mixing region for density was not calculated. This factor does not appear to have seriously affected the experimental velocity profiles other than that effect due to the interaction of the velocity and density profiles.

The theoretical velocity profiles for freon C318 and air for a λ value of 0.75 are shown in Figure IV-2-2.7. Since freon C318 is about seven times heavier than air, $\Gamma = -0.75$ and therefore the momentum of the upper and lower streams is the same. The measurements agree reasonably well with the theoretical curve for a turbulent Schmidt number of 0.5. The theoretical density profiles and the experimental data are compared in Figure IV-2-2.8. The effect of the body force on the experimental density profiles is very evident in this figure. From this data, the calculated values of the constants σ, c, and χ_1 for $\Gamma = -0.75$ and $\lambda = 0.75$ are:

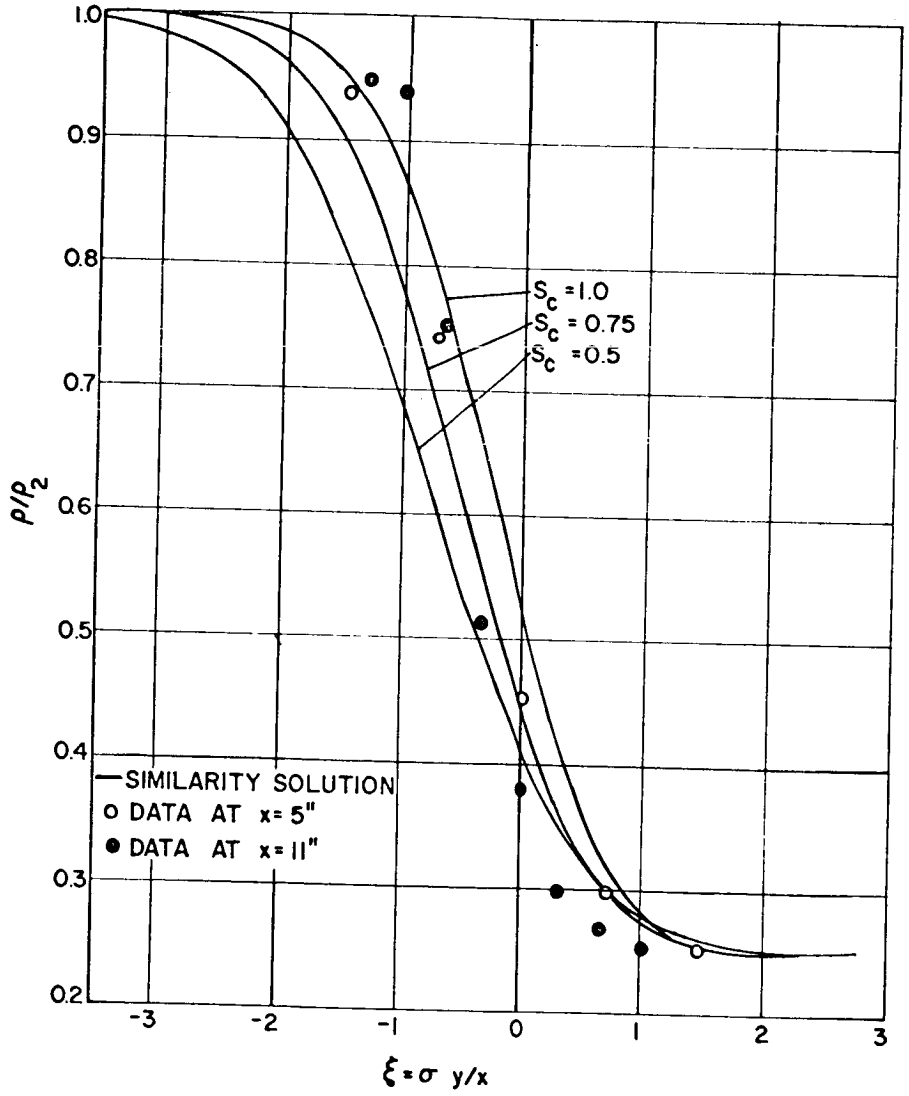

Fig. IV-2-2.4 Density Profiles of Freon 12 - Air

$\lambda = 1/3$

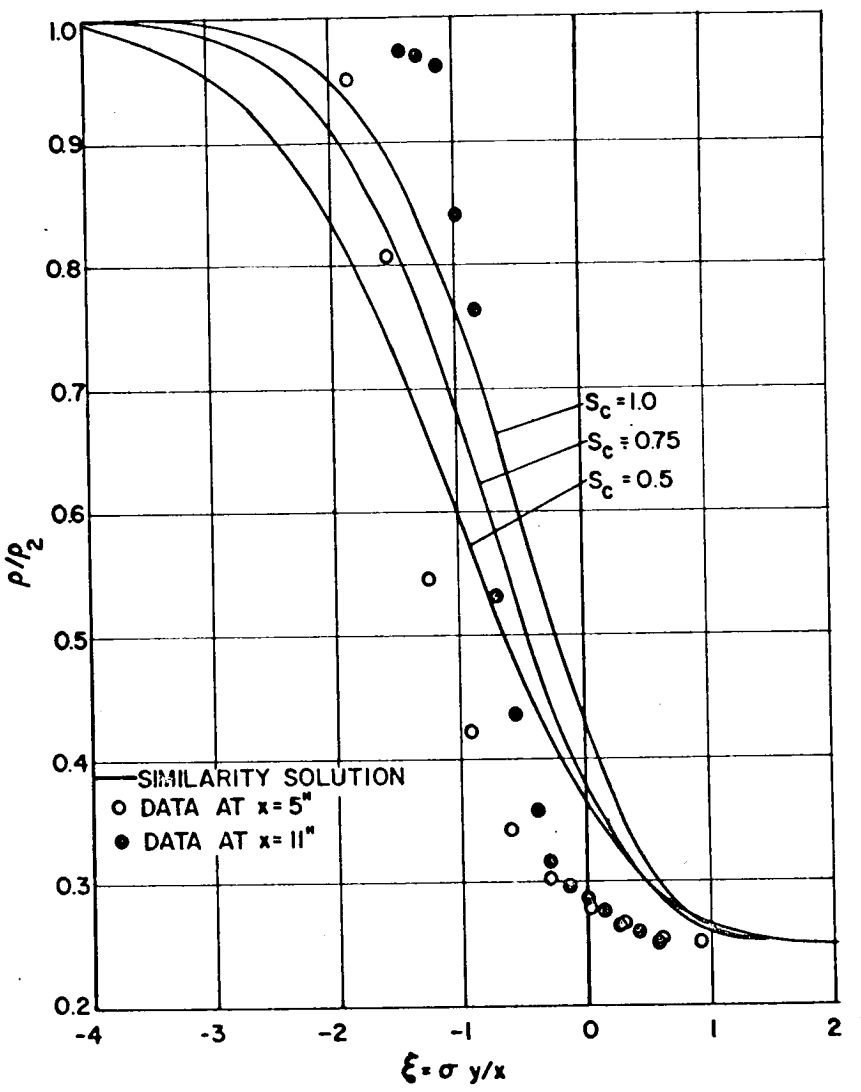

Fig. IV-2-2.5 Density Profiles of Freon 12 - Air

$\lambda = 0.6$

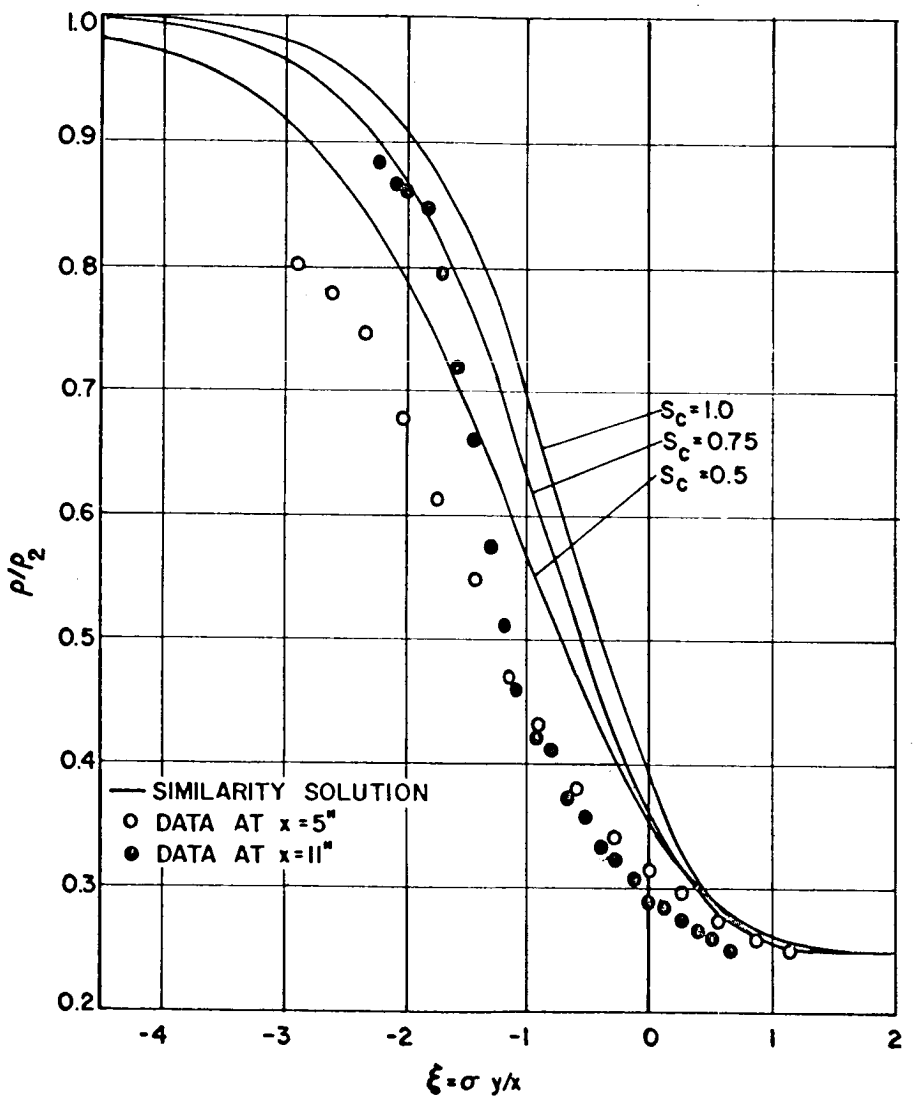

Fig. IV-2-2.6 Density Profiles of Freon 12 - Air

$\lambda = 0.8$

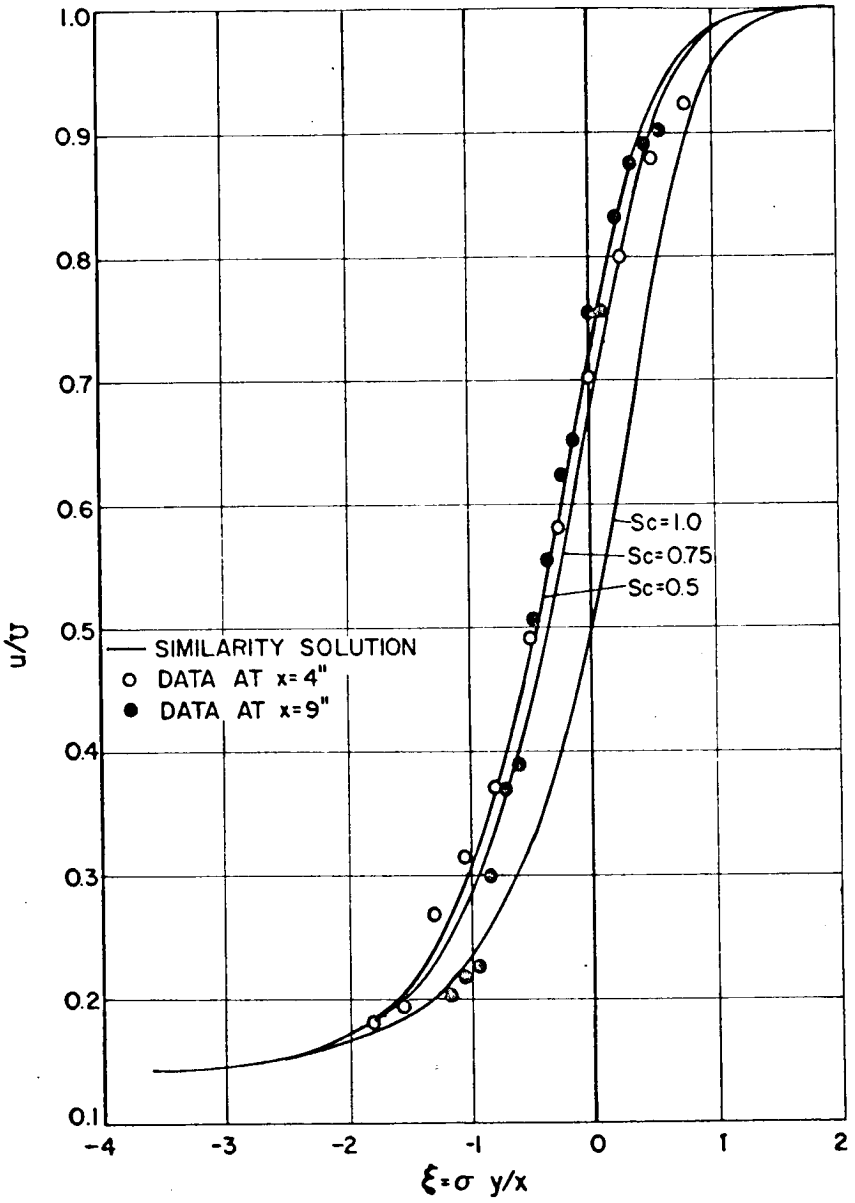

Fig. IV-2-2.7 Velocity Profiles of Freon C318-Air

$\lambda = 0.75$

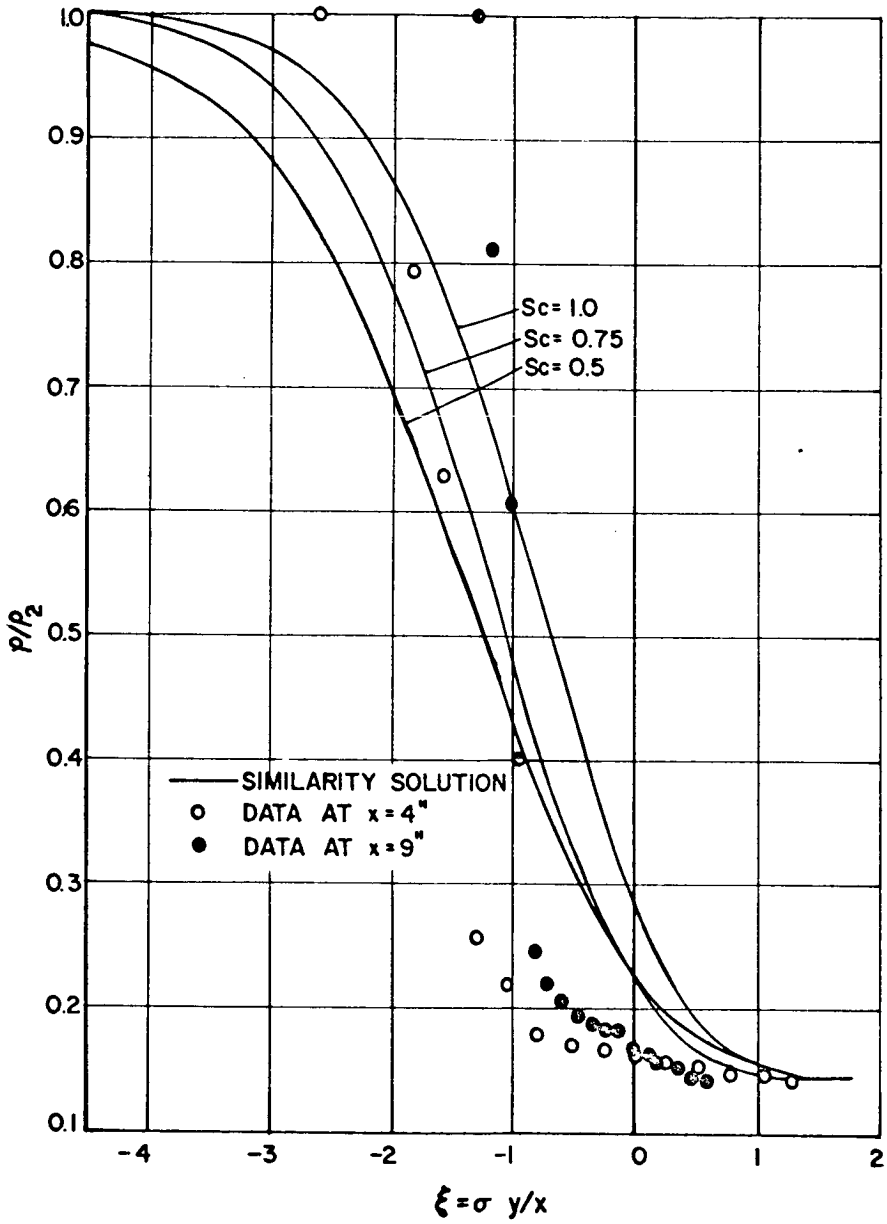

Fig. IV-2-2.8 Density Profiles of Freon C318 - Air

$\lambda = 0.75$

$\Gamma = -0.75$ $\sigma = 10.48$

$\lambda = 0.75$ $c = 0.182$

$\chi_1 = 0.0166$

The calculated values of the constants σ, c and χ_1, and the eddy viscosity ϵ are summarized in Table IV-2-2.1

Table IV-2-2-1. Summary of Calculated Constants

	σ	c	χ_1	$\epsilon = \chi_1 c \times (u_1 - u_2)$
	Homogeneous case, $\Gamma = 0$			
$\lambda = 0.2$	37.5	0.0615	0.0145	$0.000892 \times (u_1 - u_2)$
$\lambda = 0.4$	16.01	0.146	0.0167	$0.00244 \times (u_1 - u_2)$
$\lambda = 0.6$	13.75	0.173	0.0127	$0.00219 \times (u_1 - u_2)$
$\lambda = 0.8$	12.10	0.205	0.0104	$0.00213 \times (u_1 - u_2)$
$\lambda = 1.0$ (Liepmann and Laufer)	12.47	0.207	0.00775	$0.00165 \times (u_1 - u_2)$
$\lambda = 1.0$ (Albertson)	13.38	0.194	0.00719	$0.00139 \times (u_1 - u_2)$
	Heterogeneous case, $\Gamma = -0.6$			
$\lambda = 1/3$	36.9	0.0485	0.0114	$0.000553 \times (u_1 - u_2)$
$\lambda = 0.6$	15.4	0.142	0.0124	$0.00176 \times (u_1 - u_2)$
$\lambda = 0.8$	14.6	0.181	0.00810	$0.00147 \times (u_1 - u_2)$
	Heterogeneous case, $\Gamma = -0.75$			
$\lambda = 0.75$	10.5	0.182	0.0166	$0.00302 \times (u_1 - u_2)$

The following observations can be made from Table IV-2-2.1. The constant c increases with λ for all density ratios. The value of c for a given value of λ is nearly independent of Γ. Large density differences do not appreciably affect the eddy viscosity.

The theoretical affect of Γ on the velocity profiles for a constant value of λ is shown in Figure IV-2-2.9. The theoretical affect of λ on the density profiles for a constant value of Γ is shown in Figure IV-2-2.10. These figures show that if the velocity ratio is held constant, then increasing the density ratio shifts the velocity profiles toward the lighter faster moving stream. Whereas, if the density ratio is held constant, then increasing the velocity ratio shifts the density profiles toward the heavier slower moving stream.

In section IV-2-1, the theoretical effect of the value of λ on the v-velocity profiles was discussed. In this section, the theoretical effect of the density ratio and the Schmidt number on the v-velocity profiles will be illustrated. The theoretical v-velocity profiles for $\lambda = 0.6$ and various values of Γ are shown in Figure IV-2-2.11. For large negative values of ξ, the asymptotic value of v decreases with increasing density ratio. It is interesting to note that when the momentum of the two streams is the same, i.e., $-\Gamma = \lambda = 0.6$, then both asymptotic values of v are zero.

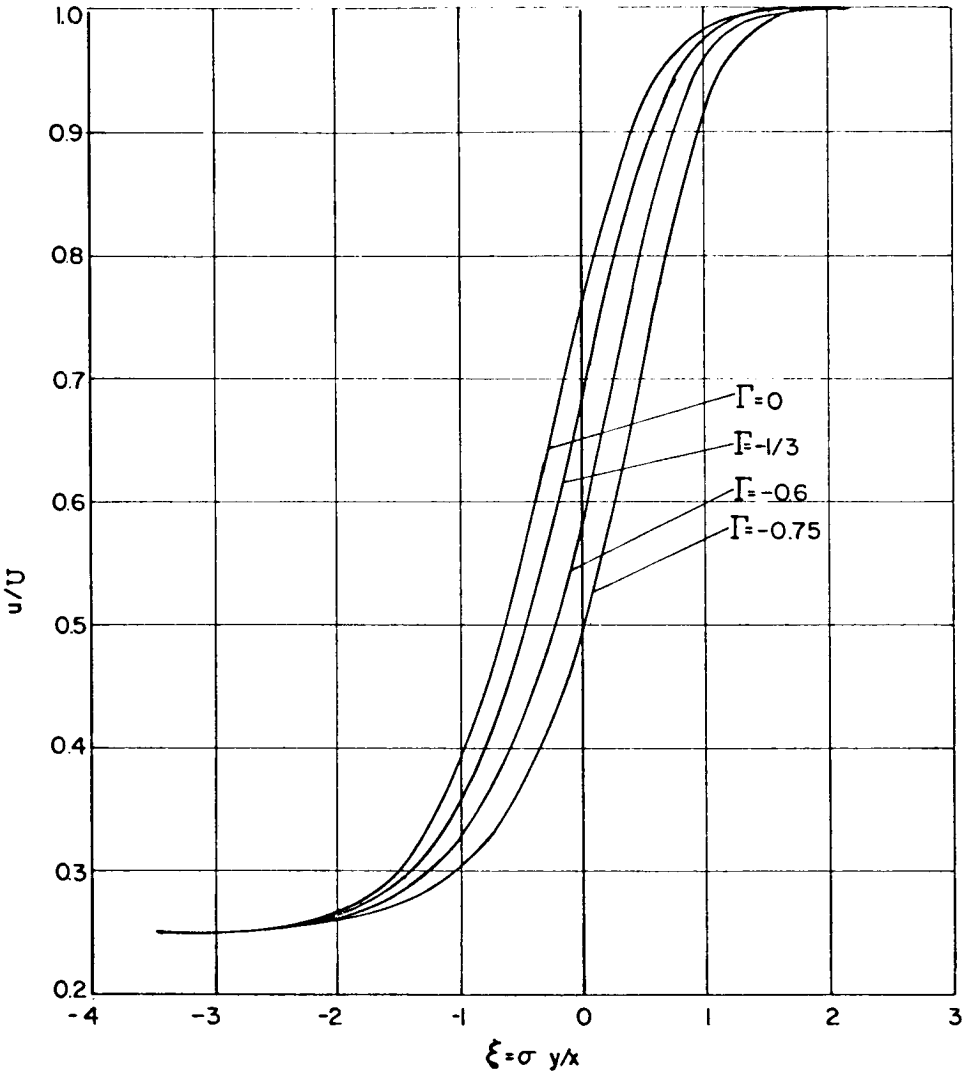

Fig. IV -2-2.9 Effect of Density Ratio
On The Velocity Profiles

$\lambda = 0.6$

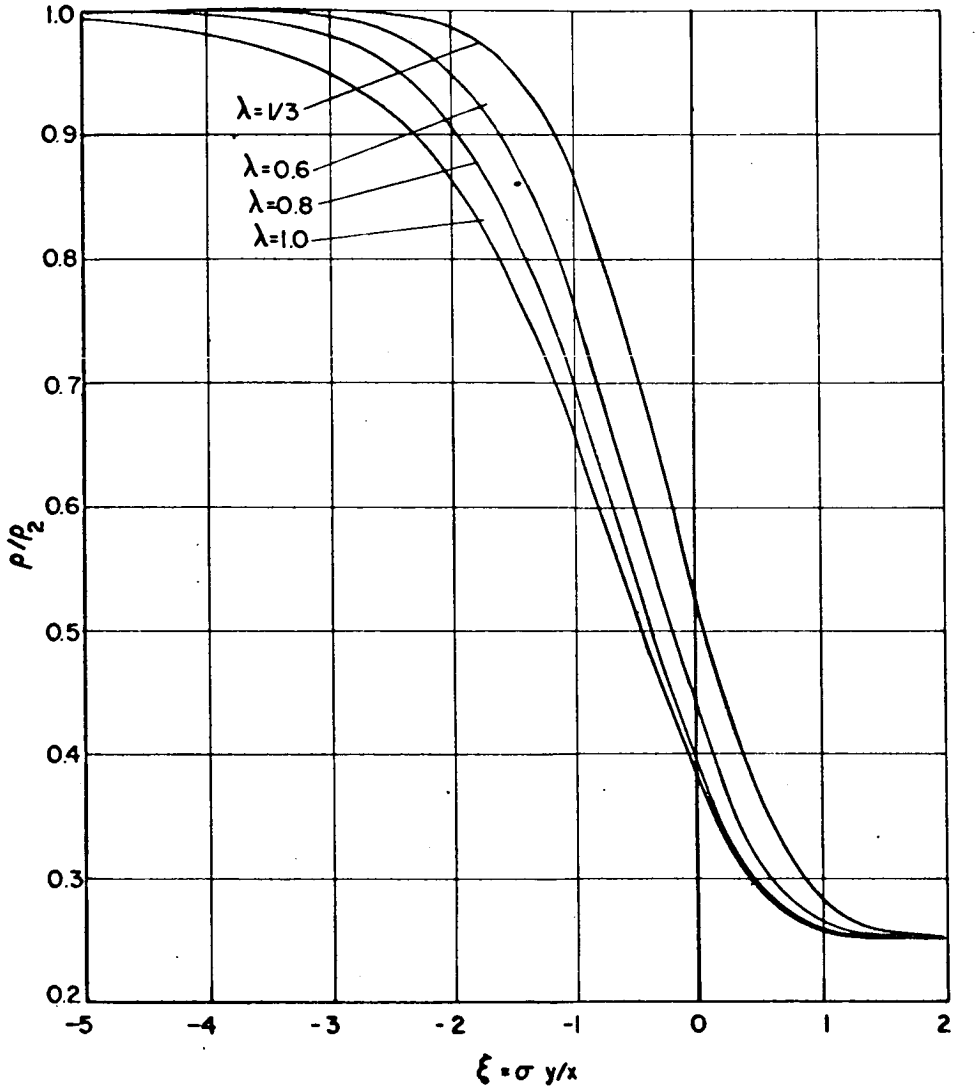

Fig. IV -2-2.10 Effect of Velocity Ratio on the Density Profiles

$\Gamma = -0.6$

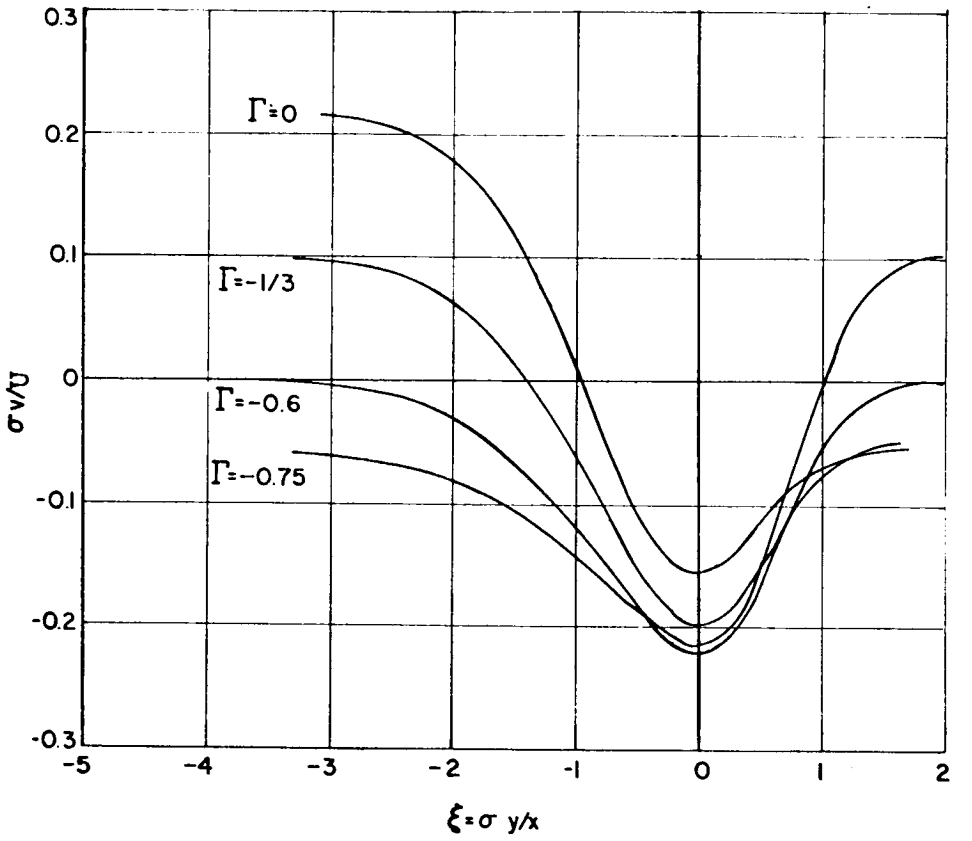

Fig. IV -2-2.11 Effect of Density Ratio on The Transverse Velocity Profiles

$\lambda = 0.6$.

The theoretical v-velocity profiles for $\lambda = 0.6$, $\Gamma = -0.6$ and various values of the Schmidt number are shown in Figure IV-2-2.12. Since $\lambda = -\Gamma$, $\rho_1 u_1 = \rho_2 u_2$. von Karman's third boundary condition for this case is

$$\rho_1 u_1 v_1 + \rho_2 u_2 v_2 = 0$$

It follows that for this case, $v_1 = -v_2$ or the asymptotic values of v at plus infinity and minus infinity are equal and opposite in sign. This is seen to be true for the theoretical velocity profiles shown in Figure IV-2-2.12. For large negative ξ, the asymptotic value of v increases as the Schmidt number is decreased and for large positive ξ the asymptotic value of v decreases as the Schmidt number is decreased. In this special case, the asymptotic values of v are equal and opposite in sign and for a Schmidt number of unity the asymptotic values are both zero.

The v-velocity profiles shown in Figures IV-2-2.11 and IV-2-2.12 are for the molar average velocity v^*. Thus, the theoretical velocities predicted in the mixing region are not directly measurable experimentally. However, the asymptotic values of v occur in a region where the fluid is pure component 1 or component 2. In this region v and v^* are identically the same.

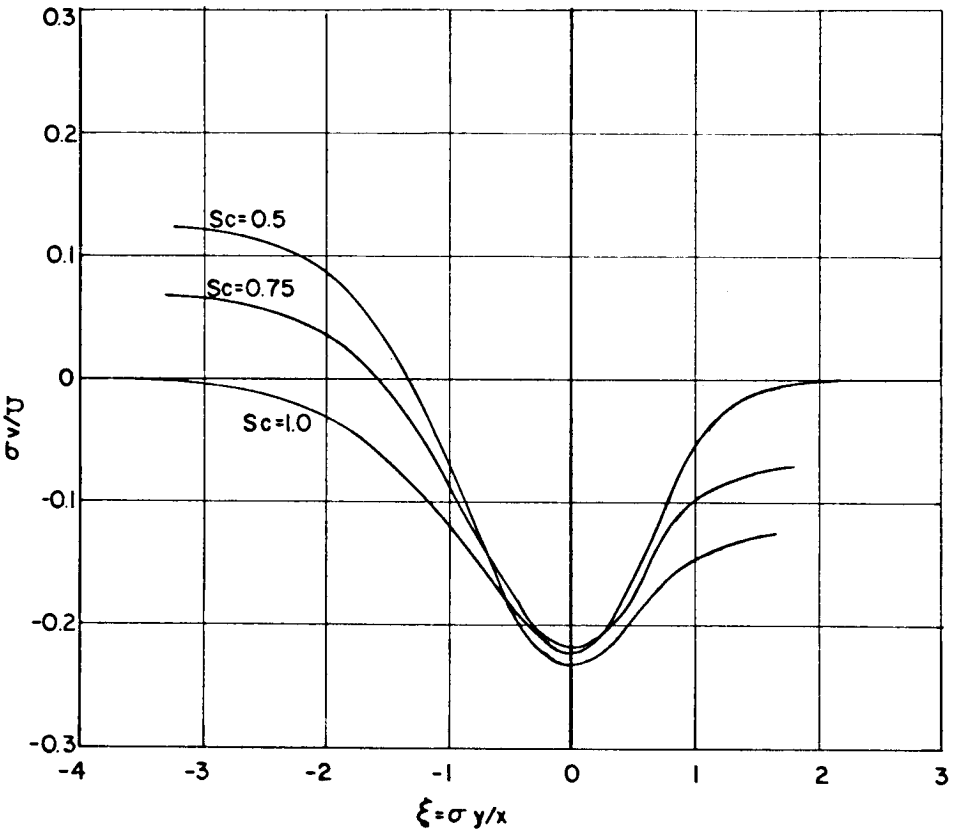

Fig. IV-2-2.12 Effect of Schmidt Number on The Transverse Velocity Profiles

$\lambda = 0.6$

$\Gamma = -0.6$

BIBLIOGRAPHY

1. Tollmien, W., Berechnung turbulenter Ausbreitungsvorgange. ZAMM 6, 458-478 (1926) NACA TM 1085 (1945).

2. Rayleigh, Lord, Science Papers I, 474 (1880)· III, 17 (1887), IV, 197 (1913).

3. Iessen, M., NACA Technical Note 929 (1950).

4. Goertler, H., Berchnung von Aufgaben der frein Turbulenz auf Grund eines neuen Naherungsansatzes. ZAMM 22, 244-253 (1942).

5. Kuethe, A., "Investigation of the Turbulent Mixing Regions Formed by Jets," J. Appl. Mech., 11, 3, A, 87, (1935).

6. Chiarulli, P., Wright-Patterson Air Force Base Headquarters Air Material Command Technical Report No. TS/1228-1A (1949).

7. Iin, C. C., NACA Technical Note 2887 (1953).

8. Szablewski, W., Zur Theorie der turbulenten Stromung von Gasen stark veranderlicher Dichte. Ing.-Arch. 20, 67 (1952).

9. Szablewski, W., Zeitliche Auflosung einer ebenen Trennungsflache der Geschwindigkeit und Dichte. ZAMM 35, 464-468 (1955).

10. Szablewski, W., Turbulente Vermischung zweier ebener Luftstrahlen von fast gleicher Geschwindigkeit und stark unterschiedlicher Temperature. Ing.-Arch. 20, 73 (1952).

11. Pai, S. I., "On Turbulent Jet Mixing of Two Gases at Constant Temperature," J. of Appl. Mech. 22, (1955).

12. Liepmann, H. W., and J. Laufer, NACA Tech. Note 1257 (1947).

13. Reichardt, H. Gesetzmassigkeiten der freien Turbulenz. VDI-Forschungsheft, 414 (1942), 2 ed. 1951.

14. Albertson, M. L., Dai, Y. B., Jensen, R. A., and Rouse, H., "Diffusion of Submerged Jets," Proc. Am. Soc. Civil engrs., 74, (1948) 1571.

15. Tollmien, W., Einallgemeines Kriterium der Instabilitat Laminarer Geschwindigkeitsverteilungen. Nachr. Gas. Wiss. Goettingen Math. Phys. Klasse, Fachgruppe I, 1, 79-114 (1935) Engl. transl. in NACA TM No. 792 (1936).

16. Lessen, M. and S. Ko, "Viscous Instability of an Incompressible Fluid Half-Jet Flow," Physics of Fluids, 9, 1179 (1966).

17. Heisenberg, W., Euber Stabilitaet und Turbulenz von Fluessigkeitsstroemen, Ann. Phys. 74, 577-627 (1924).

18. Lessen, M., Fox, J. A. and Zien, H., J. Fluid Mech. 23, 355 (1965).

19. Betchov, R. and Szewczyk, A., Phys. Fluids 6, 1391 (1963).

20. Curle, N., Aeronautical Research Council, Great Britain, Fluid Motion Sub-Committee Report F. M. 2400 (1956).

21. Esch, R., J. Fluid Mech. 3, 289 (1957).

22. Tatsumi, J., and Gotoh, K., J. Fluid Mech. 7, 433 (1960).

23. Carrier, G. F. and Chang, C. T., 1959 On An Initial Value Problem Concerning Taylor Instability of Incompressible Fluid. Quart. Appl. Math. 16, 4.

24. Menkes, J., "On The Stability of a Shear Layer", J. Fluid Mech. 6, 1959.

25. Richardson, L. F.,"The Supply of Energy From and To Atmospheric Eddies." Proc. Roy. Soc. London,A 97, 354 (1926).

26. Prandtl, L., Einfluss Stabilisierender Krafte auf Die Turbulenze. Vortrage aus d. Geb. d. Aerodyn. u. Verwandter Gebiet, Aachen 1929, 1; Springer Berlin 1930.

27. Taylor, G. I.,"Effects of Variation in Density on the Stability of Superposed Streams of Fluid." Proc. Roy. Soc. London, A132, 499 (1931).

28. Goldstein S.,"On The Stability of Superposed Streams of Fluids of Different Densities." Proc. Roy. Soc. London, A 132, 523 (1939).

29. Drazin, P. G., "The Stability of a Shear Layer in an Unbounded Heterogeneous Inviscid Fluid." J. Fluid Mech., 4, 1958.

30. Miles, J. W., "The Stability of a Heterogeneous Shear Layer," J. Fluid Mech., 6, 583 (1959).

31. Case, K. M., "Stability of an Idealized Atmosphere. I. Discussion of Results," The Physics of Fluids, 3, 149-54 (1960).

32. Dikii, L. A., "On The Stability of Plane Parallel Flows of an Inhomogeneous Fluid," PPM 24, 249-257, 1960.

33. Chandrasekhar, S.,"Hydrodynamic and Hydromagnetic Stability,"Oxford Press, 1961.

34. Menkes, J., "On The Stability of a Heterogeneous Shear Layer Subject of a Body Force," J. Fluid Mech., 11, 1961.

35. Shen; S. F., "The Theory of Stability of Compressible Laminar Boundary Layers with Injection of a Foreign Gas", NAVORD Report 4467, 28, May 1957.

36. Schlichting, H., Turbulenz bei Warmeschichtung. ZAMM 15, 313 (1935), also Proc. Fourth Int. Congr. Appl. Mech., Cambridge, p. 245, 1935.

37. Prandtl, L., Bericht uber Untersuchungen zur Ausgebildeten Turbulenz. ZAMM 5, 136 (1925).

38. Taylor, G. I., "The Transport of Vorticity and Heat Through Fluids in Turbulent Motion," Proc. Roy. Soc., (London), A-135, 828, 685 (1932).

39. Reichardt, H., "Gesetzmassigkeiten der Freien Turbulenz," VDI-Forschungsh., 414 (1951).

40. Prandtl, L., "Bemerkung zur Theories der Freien Turbulenz," ZAMM 22, 5 (1942).

41. Abramovich, G. N., The Theory of Turbulent Jets, Massachusetts Institute of Technology Press, Cambridge, Mass., 1963.

42. Prandtl, L., The Mechanics of Viscous Fluids. In W. F. Durand, Aerodynamic Theory, III, 166 (1935). See also Proc. 2nd Intern. Congr. of Appl. Mech. Zurich 1926.

43. Yen, K. T., "On the Indeterminateness of the Boundary Conditions for the Mixing of Two Parallel Streams," Transactions of the ASME, p. 390, 1960.

44. Crane, L. J., "The Laminar and Turbulent Mixing of Jets of Compressible Fluid - Part II, The Mixing of Two Semi-Infinite Streams," Journal of Fluid Mechanics, 3, 1957.

45. Torda, T. P., Ackermann, W. O. and Burnett, H. R., "Symmetric Turbulent Mixing of Two Parallel Streams," J. Appl. Mech., 20, 1953, p. 63.

46. Chapman, A. J. and Korst, H. H., "Free Jet Boundary with Consideration of Initial Boundary Layer," Proc. 2nd U. S.Nat. Cong. of Appl. Mech., 1954, p. 723.

47. Ackerman, W. O., "Laminar Incompressible Mixing of Two Streams of Different Velocities," Tech. Report No. 14-TR-4, Contract No. AF 33(038)-21251, Aug. 1952.

48. Keulegan, G. H., "Laminar Flow at the Interface of Two Liquids," U. S. Bur. Stds., J. of Research, 32, (1944), p. 303.

49. Lock, R. S., "The Velocity Distribution in the Laminar Boundary Layer Between Parallel Streams," Quarterly Journal of Mech. and Appl. Math., 4, 1957, p. 81.

50. Potter, C. E., "Laminar Boundary Layers at the Interface of Co-Current Parallel Streams," Quart. J. of Mech. and Appl. Math., 10, 1957, p. 302.

51. Kobashi, Yasiyiro, "An Experiment on Turbulent Mixing," Proc. of 3rd Japan Nat. Cong. for Appl. Mech., 1953, p. 261.

52. Sato, H., "Experimental Investigation on the Transition of Laminar Separated Layer," J. of Phys. Soc. of Japan, 11, 1956.

53. Sato, H., "Further Investigation on the Transition of Two-Dimensional Separated Layer at Subsonic Speeds," J. of Phys. Soc. of Japan, 14, 1959.

54. Hauff, K., M. S. Thesis, Illinois Institute of Technology, 1966.

55. Ellison, T. H., and Turner, J. S., "Turbulent Entrainment in Stratified Flows," J. Fluid Mech. 6, 1959.

56. Minami, I., "On The Transport of Salinity in Stratified Turbulent Flows," Pro. 12 Japan Nat. Cong. for Appl. Mech, 1962, p. 133.

57. Webster, C. A. G., "An Experimental Study of Turbulence in a Density-Stratified Shear Flow," J. Fluid Mech. 19, 1964.

58. Okuda, S., "The Velocity Distribution at the Interface Between Two Liquids," J. Phys. Soc. of Japan 16, No. 2, 1961, p. 324.

59. Reichardt, H. and Prandtl, L., Einfluss von Warmeschichtung auf die Eigenschaften einer Turbulenten Stromung. Deutsche Forschung, No. 21, 110 (1934).

60. Schlichting, H., Boundary Layer Theory, Fourth Edition, McGraw-Hill Book Company, Inc., New York, 1960.

61. Hu, N., "On Turbulent Mixing of Two Fluids of Different Densities," Ph. D. Thesis, California Institute of Technology, 1944.

62. Yiş C., Quart. Appl. Math., 12, p. 434, 1955.

63. King, L. V., Phil. Trans. Roy. Soc. London, 214A, p. 373, (1914).

64. Van der Hegge Zijnen, B. G., Appl. Sci. Research, 6A, p. 129 (1956).

65. Kramers, H., Physica, 12, p. 61 (1946).

66. Hinze, J. O., Turbulence, McGraw-Hill Book Company, Inc. (1959).

67. Baker, R. L. and Weinstein, H., "Analytical Investigation of the Mixing of Two Parallel Streams of Dissimilar Fluids." NASA CR-956.

NASA-Langley, 1968 —— 12 E-4127